KfK 3753
August 1984

Modeling Steady State and Transient Fission Gas Behaviour with the Karlsruhe Code LAKU

L. Väth
Institut für Neutronenphysik und Reaktortechnik
Projekt Schneller Brüter

Kernforschungszentrum Karlsruhe

KERNFORSCHUNGSZENTRUM KARLSRUHE

Institut für Neutronenphysik und Reaktortechnik
Projekt Schneller Brüter

KfK 3753

Modeling Steady State and Transient Fission Gas Behaviour with the Karlsruhe Code LAKU

L. Väth

Kernforschungszentrum Karlsruhe GmbH, Karlsruhe

Kernforschungszentrum Karlsruhe GmbH
ISSN 0303-4003

Abstract

The programme LAKU models the behaviour of gaseous fission products in reactor fuel under steady state and transient conditions, including molten fuel. A presentation of the full model is given, starting with gas behaviour in the grains and on grain faces and including the treatment of release from porosity. The results of some recent calculations are presented.

Modellierung des Spaltgasverhaltens unter stationären und transienten Bedingungen mit dem Karlsruher Code LAKU

Zusammenfassung

Das Programm LAKU modelliert das Verhalten gasförmiger Spaltprodukte im Reaktorbrennstoff unter stationären und transienten Bedingungen unter Einbeziehung eines Modells für geschmolzenen Brennstoff. Das gesamte Modell wird vorgestellt, beginnend mit dem Gasverhalten in Körnern und auf Kornoberflächen bis zur Behandlung der Freisetzung aus der Porosität. Am Schluß werden die Ergebnisse von kürzlich durchgeführten Rechnungen präsentiert.

Contents

1. Introduction

Reactor fuel pin behaviour under steady state and transient conditions is in part determined by the behaviour of the gaseous fission products. Those retained in the fuel matrix contribute to fuel swelling and may, under transient conditions, determine time and mode of pin failure and fuel movement. Gases released from the matrix influence internal pin pressure and fuel-cladding gap conductance. Therefore, considerable effort is being put into modeling all aspects of fission gas behaviour.

The Karlsruhe code for treating these problems, LAKU, is the result of improving and extending an older code, LANGZEIT/KURZZEIT /1/. The changes are so numerous that a complete documentation of the new code is in order. However, a detailed presentation of all models contributing to the code would be far too extensive, resulting only in a repetition of older publications. Therefore, as far as possible, no deductions of formulas will be presented, referring the reader to the corresponding literature instead.

Concerning the amount of detail modeled, LAKU must be counted among the more sophisticated codes. Nevertheless, it contains one important simplification: Instead of dividing the bubbles into groups according to size, as do the most detailed codes (e.g. /3/), only one group with an average bubble radius is used. This simplification leads to considerably reduced computer times and makes the code suitable for insertion into more comprehensive programs such as pin behaviour models. In this respect, LAKU is comparable to a number of detailed models employing the same approximation (e.g. /4,5/).

Two versions of LAKU are available. The stand-alone version is the more comprehensive one - though modeling of a few effects is lacking to date - and thus the slower and costlier. By employing a number of simplications and approximations, a fast version has been developed, which is suitable for coupling to a pin behaviour model such as URANUS /2/. This report deals with the full version, leaving the documentation of the coupled code URANUS-LAKU to a separate publication.

The next chapter will briefly present the two equations of state for the fission gases in cavities, which are currently realized in LAKU. Then,

three chapters are devoted to modeling the gas behaviour in the grains, on grain faces, and in the fabricated and sintering porosity under the assumption, that the grains can be idealized as spherical. An extra chapter summarizes the changes to be made to the formulas, when this assumption is dropped for growing grains, an option that has been introduced recently. A chapter on the gas model for molten fuel finishes the presentation of theory. The last chapter deals with the material constants employed by the code, and presents the results of a few calculations.

2. Equation of State

The equation of state for the fission gas in bubbles and cavities is common to many parts of the programme and is therefore put at the beginning of the model description. Two equations of state are realized in LAKU. The normal option is the reduced Van-der-Waals equation:

$$\frac{b}{n} RT = (\alpha r^3 - \frac{b}{n} w) \left(\frac{2\gamma \sin\psi}{r} + p + p_{ex} \right) \qquad (2.1)$$

$\frac{b}{n}$ gas content of bubble in moles

R universal gas constant

T temperature

r bubble radius

w Van-der-Waals constant

γ surface tension of fuel

ψ contact angle of grain boundary bubble

p local hydrostatic pressure

p_{ex} excess pressure in bubble. $p_{ex} = 0$ for equilibrium bubble.

This form of (2.1) is suitable for spherical bubbles as well as the lenticular bubbles occurring on grain faces (see Fig. 1). For the two different bubble geometries:

	spherical	lenticular
$\sin\psi$	$\sin \frac{\pi}{2}$	$\sin 50°$
α	$\frac{4\pi}{3}$	$\frac{2\pi}{3} \frac{(1-\cos\psi)(2+\cos\psi)}{\sin\psi(1+\cos\psi)}$

(2.2)

Optionally, (2.1) may be replaced by an improved equation of state, which is more correct for the high gas densities and pressures occurring in the small intragranular bubbles. It reads /6/

$$\frac{b}{n} RT \frac{1+y+y^2-y^3}{(1-y)^3} = \alpha r^3 \left(\frac{2\gamma \sin\psi}{r} + p + p_{ex} \right)$$

$$y = \frac{\pi}{6\alpha} \frac{b}{n} L \left(\frac{d}{r} \right)^3 \qquad (2.3)$$

$$d = (3.80119 - .177822 \ln \frac{T}{231.2}) \cdot 10^{-8} \quad d[\mathrm{cm}], \quad T[\mathrm{K}]$$

L Avogadro's number

For low pressures, this equation reduces to the reduced Van-der-Waals equation /6/.

In LAKU, the equation of state has to be solved for either of the three variables b, p_{ex}, or r. Calculation of $p_{ex}(b,r)$ and $b(p_{ex},r)$ is straightforward for (2.1); the iterative scheme used for the derivation of $r(p_{ex},b)$ from (2.1) has been described in /1/. When (2.2) is employed, only $p_{ex}(b,r)$ can be quickly calculated. For the calculation of $b(p_{ex},r)$ and $r(p_{ex},b)$ from (2.2), the same kind of iteration (Newton-Raphson) is used as for (2.1); the first guesses are, for $b(p_{ex},r)$, the solution of the Van-der-Waals equation, and for $r(p_{ex},b)$, the same guess as that used for the Van-der-Waals equation /1/. Normally, very few iterations are needed for convergence.

The kind of equation of state used directly affects the running times of the code, since it is referred to in the innermost part of the iterations. Obviously, (2.2) is the more elaborate formula. It is seldom used in practice, since its effects on overall gas behaviour are small, but computer times go up by about 50 % as compared to the reduced Van-der-Waals equation.

3. Intragranular Gas

The models describing the behaviour of fission gases in the grains until they are released to the grain surface are slightly different depending on whether steady state or transient conditions are to be modeled. Under stationary conditions, restructuring plays an important role; this can be neglected in modeling transients, for which intragranular bubble migration is the dominant mechanism. Starting from atomic gas being formed in the fuel matrix, the following processes are included:

A. Formation and destruction of intragranular bubbles during irradiation.

B. Precipitation of gas into intragranular bubbles. The resolved fission gas diffuses in the fuel matrix and at higher temperatures tends to collect in bubbles, as is known from experimental evidence. As an important simplification, the model assumes all bubbles to be of equal size and to contain an equal amount of gas. Under steady state conditions, the bubbles are assumed to have their equilibrium volume, an assumption that has to be abandoned for the transient part.

C. Resolution of gas from bubbles. Interaction of bubble gas with energetic fission products causes it to be redissolved in the fuel matrix.

D. Diffusion of resolved gas to the surface of the grain.

E. Migration of gas bubbles to the surface of the grain. The gas bubbles are immobile at temperatures up to 1500°C /7/, but beyond that start to move in a temperature gradient. Modeling this process is very important under transient conditions, but is included in a simplified way in the stationary part of LAKU too, since it contributes to gas release at higher irradiation temperatures.

F. Coalescence of migrating bubbles.

G. Time dependent bubble volume equilibration by vacancy diffusion (including vacancy depletion) and high temperature creep enhancement. Since instantaneous volume equilibration is assumed for irradiation conditions, this process is treated under transient conditions only.

H. Sweeping processes. Fission gases are swept from the grains by grain boundaries moving due to grain growth, and by pores moving through the material up a temperature gradient. At high irradiation temperatures, these processes may contribute significantly to gas release /8,9/. They are not included in the transient part, but sweeping of the resolved gas by the moving intragranular bubbles is.

The grains in the unrestructured fuel are idealized as spherical. Originally, this assumption was used for the growing grains, too. As has been stated in the introduction already, spherical grains will be assumed throughout this chapter, since formulas tend to become unnecessarily complicated for the elongated grain model. The changes introduced by this model will be summarized in chapter 6. All grains contained in one radial subzone of a pin section are assumed to have the same diameter.

The equations governing the processes listed above will now be presented for each process separately. In the end, they will be joined together to form the complete set of equations for the intragranular gas under stationary or transient conditions. The gas components are denoted as

c	intragranular resolved gas	[moles/cm³]
b	intragranular bubble gas	[moles/cm³]
g	gas released from grains	[moles/cm³]

A. Formation and loss of bubbles

This process is currently treated by postulating a fixed number of uniformly distributed possible bubble sites and then explicitly modeling the processes leading to bubble formation at these sites, and to losses. Bubble formation is assumed to take place, if one gas atom that already resides at such a site is joined by a second one before diffusing away. Thus

$$\dot{n}_{form} = (n_o - n) \cdot 4\Omega c L \cdot 4\pi D_g r_o c L \qquad (3.1)$$

n_o	number density of bubble sites
n	number density of existing bubbles
Ω	molecular volume

D_g intragranular diffusion coefficient of atomic gas
r_o radius of site

In (3.1), the first term on the right hand side is the number of sites available for the formation of new bubbles; the second is the probability for one gas atom to reside at the site; the third one is the probability per unit time for a second gas atom to be precipitated to the site, and is derived from the precipitation term in subsection B (see 3.6). For the derivation of the second term, the site has been assumed to have a volume of 4Ω, and from this assumption:

$$r_o = \sqrt[3]{\frac{3\Omega}{\pi}} \tag{3.2}$$

Bubble losses occur by resolution, sweeping processes, and bubble migration and coalescence:

$$\dot{n}_{loss} = -(\eta+f+2\pi nr^2v+8\pi nD_b r)n \tag{3.3}$$

η resolution constant
f relative intragranular bubble losses (per unit time) by sweeping and bubble migration (see 3.34) (steady state part only)
v intragranular bubble velocity
D_b bubble diffusion coefficient

The last two terms in (3.3) describe the reduction in bubble number density due to coalescence caused by both biased and random migration (see subsection F).

From (3.1) - (3.3):

$$\dot{n}_{form} + \dot{n}_{loss} = \dot{n} = (n_o-n)WD_g c^2-Vn \tag{3.4}$$

$$W = 16\Omega L^2 \sqrt[3]{3\pi^2\Omega}$$

$$V = \eta+f+2n(0)r^2v$$

Here, n(0) has been substituted for n in the coalescence term in order to get rid of the nonlinearity in (3.3). This can be done, since (3.4) is

solved for comparatively short time intervals, and then updated. The solution of (3.4) is

$$n(t) = n(0)\exp(-(WD_g c^2+V)t) + n_o \frac{WD_g c^2}{WD_g c^2+V} \cdot (1-\exp(-(WD_g c^2+V)t)) \qquad (3.5)$$

In LAKU, the total irradiation interval is divided up into subintervals, for which the differential equations describing the evolution of the gas components (b,c) are integrated numerically. (3.5) is evaluated before each subinterval, the evolution of the bubble number is linearized and fed to the integration routine. This procedure is faster than including (3.4) among the differential equations, and sufficiently accurate.

At low temperatures, n(t) gradually approaches n_o, which should thus be chosen to represent measured bubble densities. At higher temperatures, most of the gas tends to precipitate into already existing bubbles, and thus bubble densities remain considerably lower than n_o; this is in accordance with post irradiation examination results, which indicate grains to be essentially denuded of bubbles at higher temperatures (e.g. /8/).

The equation for transient bubble number density is given at the end of this chapter.

B. Precipitation

This process is described by the diffusion equation. The bubbles are assumed to be uniformly distributed through the grain volume (under transient conditions: the part of the grain, that has not been swept clean of bubbles by bubble migration). Each bubble can then be assigned an equal share of solid material surrounding it, which contains an equal amount of resolved gas. If this volume is idealized as a sphere, the gas diffusion equation can be easily solved, employing the proper boundary conditions /10/. From the solution, the rate of gas precipitating into bubbles results as

$$\dot{b}_{prec} = 4\pi D_g nrc \qquad (3.6)$$

C. Resolution

This process results from the interaction of the energetic fission products with the gas bubbles. It is alternately described as a single gas atom being reinjected into the fuel matrix after colliding with a fission fragment /11/; or as a whole bubble being destroyed in the wake of a fission product crossing it /12/. Since a resolution parameter has to be postulated for either model, and since this parameter is not known very well at present, a simple description is employed in LAKU:

$$\dot{b}_{resol} = -\eta b \qquad (3.7)$$

This equation corresponds to the second model, but is valid for the first model, too, in the case of small bubbles.

D. Diffusion of atomic gas to the surface of the grain

Like precipitation into bubbles, this process is governed by atomic gas diffusion and, if the grain is idealized as a sphere, the diffusion equation describing it is the same; only boundary conditions and dimensions are different. The important difference is the dimension. For a bubble density of $10^{16}/cm^3$, the radius of the sphere surrounding the bubble is about $3 \cdot 10^{-6}$ cm, whereas typical grain radii are two orders of magnitude bigger. The analytic solution of the diffusion equation for the precipitation problem can be truncated to the first term, since higher modes die out quickly. This cannot be done for the grain boundary release problem at least at low temperatures, for which the relaxation constant is typically of the order of years. Thus, any approximate solution must be carefully tested as to whether it is able to describe all possible situations, especially changing reactor operating conditions. A numerical solution /13/ is well suited to the problem, but somewhat too cumbersome for a code like LAKU. Therefore, an analytic approximation was developed /14/, which employs an estimate of the instantaneous time constant for the actual gas concentration approaching the asymptotic one:

$$c_{as}(t) = \frac{\beta(t)a^2(t)}{15D_g(t)}$$

$$\frac{dc(t)}{dt} = \omega(t,\tau)\left(\frac{\beta(t)a^2(t)}{15D_g(t)} - c(t)\right) \tag{3.8}$$

$$\frac{d\tau(t)}{dt} = \frac{D_g(t)}{a^2(t)} \tag{3.9}$$

$$\omega(t,\tau) = \frac{D_g(t)\pi^2}{a^2(t)}\left(\sum_{n-1}^{\infty}\frac{1}{n^2}\exp(-n^2\pi^2\tau)\right)\left(\sum_{n=1}^{\infty}\frac{1}{n^4}\exp(-n^2\pi^2\tau)\right)^{-1}$$

a grain radius

β gas production rate $[\text{moles/cm}^3\cdot\text{s}]$

When (3.8) is combined with the equations describing precipitation, resolution, and sweeping, β has to be replaced by an effective value, which is corrected for the gains and losses due to these effects. $\omega(t,\tau)$ is the instantaneous relaxation constant which contains, for low values of τ, the contributions of the higher spatial modes - the $n > 1$-terms in the two series. For increasing τ, these terms vanish. τ is normally continuously integrated even after temperature changes, but may be reset to zero, if an abrupt change to considerably lower temperatures occurs. Then, the asymptotic concentration has to be built up from a practically zero value. This situation is identical to a fresh start and must thus be simulated with a period ω containing all higher modes, i.e. corresponding to the τ=0-conditions.

E. Bubble migration

This process plays a dominant role under transient conditions, but is only of moderate importance under irradiation conditions, and then only for high temperatures. It is thus treated in very different ways in the two parts of the program. The formalism for the transient part will be presented first, since the stationary treatment is essentially a gross simplification of the transient one.

Under transient conditions, the bubbles can migrate under the influence of a temperature gradient due to surface diffusion of the matrix atoms. For surface diffusion /15/:

$$D_b = \frac{6\Omega^{4/3} D_s f(r)}{\pi r^2 \lambda^2} \qquad (3.10)$$

$$f(r) = 1 \qquad r \leq \lambda/\pi$$

$$= \sin^2(\lambda/2r) \qquad r \geq \lambda/\pi$$

D_b intragranular bubble diffusion coefficient
D_s surface diffusion coefficient
λ mean jump distance of surface atom

The resulting bubble velocity is /15/

$$v = \frac{4\pi r^3}{3\Omega} \frac{Q_s \nabla T_s D_b}{kT^2} \qquad (3.11)$$

$$= \frac{8\Omega^{1/3} r f(r) Q_s \nabla T_s D_s}{\lambda^2 kT^2}$$

$$= \frac{2\Omega^{1/3} Q_s \nabla T_s D_s}{rkT^2} \qquad \text{for } r >> \frac{\lambda}{\pi}$$

Q_s surface diffusion heat of transport
∇T_s thermal gradient at bubble surface

$$\nabla T_s \simeq \frac{3}{2} \nabla T \qquad (3.12)$$

∇T bulk thermal gradient
k Boltzmann's constant

The fraction of bubbles removed from the grain by this biased migration is calculated with Gruber's formalism (/15/; see Fig. 2):

$$F_b = \frac{s}{4a}\left(3 - \frac{s^2}{4a^2}\right) \qquad s \leq 2a \qquad (3.13)$$

$$= 1 \qquad s \geq 2a$$

s distance travelled by bubbles till transient time t,

$$s = \int_0^t v(t')dt'$$

When bubbles start to become mobile, random migration contributes somewhat to bubble release. The fraction of bubbles released by this mechanism is approximately /15/:

$$F_r = 6\sqrt{\tau_b/\pi} - 3\tau_b \qquad (3.14)$$

$$\tau_b = \int_0^t \frac{D_b(t')dt'}{a^2}$$

The total release fraction is calculated approximately from (3.13), (3.14) /15/:

$$F = F_r \qquad F_r \geq 2F_b$$

$$F = F_b + F_r/2 \qquad F_r \leq 2F_b \qquad (3.15)$$

$$F = 1 \qquad F_b + F_r/2 > 1$$

F fraction of intragranular bubbles released to grain surface

In the transient part of LAKU, the differential equations for precipitation, resolution, and bubble coalescence are integrated, as if the bubble field would not move relative to the grain. The bubble number density has thus the value for the region not yet denuded of bubbles by migration. (3.15) is applied after the integration of the differential equations to determine the fraction of bubbles remaining in the grain. The situation is somewhat different for steady state conditions.

Under irradiation conditions, only the innermost pin zones may reach temperatures high enough for bubble migration to play a significant role. In addition, bubbles may be faceted under equilibrium conditions and therefore move more slowly through the solid than under transient conditions. Using a steady state bubble diffusion coefficient based on measurements and some fitting of data /3/, the bubble velocity under these conditions may again be calculated from (3.11). When deducing the steady state gas release from this mechanism, the formation of new bubbles inside the grain must be taken into account. Therefore, the picture used for the derivation of (3.13), Fig. 2, is not appropriate, since the area denuded of bubbles by migration is filled up by newly formed ones. If the bubbles are assumed to be uniformly distributed through the grain, the fraction released in a small time interval Δt is:

$$\Delta F = \left.\frac{dF_b}{ds}\right|_{s=0} v\Delta t = v\Delta t \, \frac{3}{4a}$$

Random migration is neglected, because its contribution can be shown to be negligible at all temperatures. The decrease of bubble number density and intragranular bubble gas due to steady state bubble migration is deduced from this:

$$\left(\frac{\dot{n}}{n}\right)_{migr} = \left(\frac{\dot{b}}{b}\right)_{migr} = \frac{\Delta F}{\Delta t} = \frac{3v}{4a} = K\,\frac{r}{a} \qquad (3.16)$$

$$K = \frac{\pi Q_s \nabla T_s D_{b0}}{\Omega k T^2}$$

$$D_b = D_{b0}/r^2 \qquad \text{for steady state bubble diffusion.}$$

(3.16) is part of the steady state differential equations for intragranular gas and the equations governing the changes of intragranular bubble number densities (see 3.A and 3.H).

F. Bubble coalescence

Apart from gas release, bubble movement entails bubble coalescence. For two groups of bubbles with radii r_1, r_2, velocities v_1, v_2, number densities n_1, n_2, and diffusion coefficients D_{b1}, D_{b2}, the number of coalescences occurring in time interval Δt is /15/:

Biased migration:

$$G_{12} = n_1 n_2 \pi (r_1+r_2)^2 |v_1-v_2| \Delta t \qquad (3.17)$$

Random migration:

$$G_{12} = n_1 n_2 4\pi (D_{b1}+D_{b2})(r_1+r_2)\Delta t \qquad (3.18)$$

For the one-bubble-group representation used by LAKU, (3.17) and (3.18) have to be approximated by

$$G_b = \frac{n^2}{2} 4\pi r^2 v C_1 \Delta t \qquad (3.19)$$

$$G_r = \frac{n^2}{2} 16\pi D_b r C_2 \Delta t \qquad (3.20)$$

The correction factors C_1 and C_2 have been introduced to account for the effect of the actual size distribution. For transient conditions, using (3.10) and (3.11), one gets for the decrease of bubble number density due to random and biased migration:

$$\dot{n}_{co} = - \frac{16\pi\Omega^{1/3} r^3 f(r) n^2 D_s Q_s \nabla T_s C_1}{\lambda^2 k T^2} - \frac{48\Omega^{4/3} f(r) n^2 D_s C_2}{\lambda^2 r} \qquad (3.21)$$

The correction factors are taken form the work of Ostensen /5/, who analyzed bubble size distributions:

$$C_1 = \frac{1}{2}\left(1.61 - 2.49 \frac{pr}{3pr+4\gamma}\right)$$

$$C_2 = 1.6 \qquad (3.22)$$

In the steady state part, the decrease in bubble number density due to coalescence is accounted for in the last two terms of (3.3), which can be easily deduced from (3.19) and (3.20). Since the analysis by Ostensen does not apply for the steady state case with continuous bubble recreation, C_1 and C_2 are omitted; their values are near 1 anyway, as is obvious from (3.22). Random migration is accounted for, but its contribution to coalescence rates is very small.

G. Bubble volume equilibration

Bubble coalescence and increasing temperatures are the cause of bubble overpressure, which is relieved by creep processes. Under steady state conditions, instantaneous volume equilibration may be assumed for the small intragranular bubbles, but for transients, the creep processes are often slower than the pressure buildup. Therefore, the transient change of bubble radius has to be explicitly modeled in LAKU. Its four contributions are due to coalescence, precipitation and sweeping of atomic gas, and two creep processes

$$\dot{r} = \dot{r}_{co} + \dot{r}_{pr} + \dot{r}_{c1} + \dot{r}_{c2} \tag{3.23}$$

$\dot{r}_{co}$ follows from the assumption, that total bubble volume is conserved upon coalescence:

$$\dot{r}_{co} = -\frac{r}{3}\frac{\dot{n}}{n} \tag{3.24}$$

Gas precipitated into the bubble or swept up during bubble migration is assumed to be associated with one vacancy. From (3.6) and (3.33):

$$\dot{r}_{pr} = \frac{\Omega L c}{4r}\,(4D_g + rv) \tag{3.25}$$

Creep processes are caused by vacancy diffusion and, at higher temperatures, dislocation climb and glide. As is done in many codes, the first process is modeled explicitly in LAKU, including the effects of vacancy depletion. The second process is incorporated via the measured stress-strain relations.

According to Greenwood et al. /18/, and Matthews and Wood /42/

$$\dot{r}_{c1} = \frac{D_u \Omega p_{ex}}{rkT} \frac{r_z}{r_z - r} \cdot \frac{1}{1 + \frac{2a}{3}\sqrt{\pi n r}} \qquad (3.26)$$

D_u self diffusion coefficient of heavy species in grain
$2r_z$ mean distance between bubbles

$$r_z = \sqrt[3]{r^3 + \frac{3}{4\pi n}}$$

High temperature creep is assumed to be given by a relation

$$\dot{\varepsilon}_e = \sigma_e^m C \exp(-H/kT) \qquad (3.27)$$

ε_e, σ_e effective strain and stress
m, K, H experimentally determined parameters

Following the analysis of Ronchi /9/ for stress relaxation in the subcell surrounding a small bubble, the growth in bubble radius results are

$$\dot{r}_{c2} = r \frac{C}{2} \exp(-H/kT) \left[\frac{\frac{3}{2m} p_{ex}}{(r_z/r)^{3/m} - 1} \right]^m \qquad (3.28)$$

H. Sweeping processes

There are various mechanisms resulting in the entrainment of intragranular gas - resolved and/or in bubbles - and enhancing release to the grain surface. Some mechanisms can be estimated to contribute only insignificantly under both steady state and transient conditions. The three processes currently modeled by LAKU are operative only in either the steady state or the transient part. They are:

Grain boundary sweeping. Intragranular bubbles and resolved intragranular gas are swept up by the grain boundaries migrating due to grain growth processes /9/. Currently, LAKU employs a grain growth law /20/ together with a maximum condition on the grain radius /21/:

$$a^4 = a_o^4 + t a_1 \exp(-a_2/T) = a_o^4 + S^* t \qquad (3.29)$$

$$a_{max} = a_3 \exp(-a_4/T)$$

a_o grain radius of fabricated fuel
a_1-a_4 experimentally determined parameters

Then, the sweeping effect on intragranular gas content and bubble number density is /9/:

$$\left.\frac{\dot{b}}{b}\right|_{gb} = \left.\frac{\dot{c}}{c}\right|_{gb} = \left.\frac{\dot{n}}{n}\right|_{gb} = -\frac{3S(1-P)}{4a^4} \qquad (3.30)$$

P fuel porosity (fabricated/restructured)

These terms occur only in the steady state equations. Under transient conditions the time is assumed to be too short for any appreciable grain growth.

Sweeping due to pore motion. Bigger pores may start to move through the fuel matrix in a temperature gradient due to a vaporization-recondensation effect, trapping the resolved gas and small fission gas bubbles they encounter. At higher temperatures, this effect can be demonstrated to contribute significantly to intragranular gas release. The related equations are

$$\left.\frac{\dot{b}}{b}\right|_{ps} = \left.\frac{\dot{c}}{c}\right|_{ps} = \left.\frac{\dot{n}}{n}\right|_{ps} = -n_p \sigma_p v_p \qquad (3.31)$$

n_p number density of pores
σ_p sweeping cross section of the pore
v_p pore velocity

The pore velocity due to the vaporization-recondensation effect is given by /22/

$$v_p = \frac{15\Omega p_s H_s \nabla T r_{peff}}{2\ \sigma\gamma T} \sqrt{\frac{L}{2\pi kT}\left(\frac{1}{m_g} + \frac{1}{m_f}\right)} \qquad (3.32)$$

p_s equilibrium vapour pressure of fuel
H_s vaporization energy of fuel
r_{peff} effective pore radius
σ collision cross section of fuel vapour phase
m_g atomic number of pore gas
m_f molecular number of fuel

(3.32) contains a number of approximations. Therefore, $r_{p,eff}$ is used as calibration parameter for obtaining the measured pore velocities shown by Nichols /22/. Of course, r_{peff} and σ_p should be representative of the dimensions of the elongated pores observed in the equiaxed grain region.

Again, times are assumed to be too short under transient conditions for a significant contribution of this effect.

Sweeping by intragranular bubbles. When the intragranular bubbles themselves start to move, they trap all resolved gas in their path. This effect can be neglected under irradiation conditions, since equilibrium bubbles become mobile at high temperatures only, for which practically no resolved gas is left in the matrix. The situation is different in a transient, when bubbles from the unrestructured zone may start to move, before all resolved gas has been precipitated into them. Their sweeping effect is (see (3.11)):

$$\dot{b}\Big|_{bs} = -\dot{c}\Big|_{bs} = cn\pi r^2 v = cn\,\frac{8\pi\Omega^{1/3} r^3 f(r) Q_s \nabla T_s D_s}{\lambda^2 k T^2} \qquad (3.33)$$

This completes the intragranular equations. They will now be summarized separately for the steady state and transient case.

Under steady state conditions, consecutive irradiation intervals may be defined which may differ in gas production rate β, temperature T, and internal pin pressure $p_{pin} = p$; p may be a linear function of time in the interval. Each interval is internally divided into a number of subintervals, which grow in length. At the start of the calculations for a subinterval, the number density of intragranular bubbles at the end of the

subinterval is extrapolated via (3.5) from the conditions at the start of the subinterval, and then linearized. Then, the following differential equations are integrated with a Runge-Kutta-method (see (3.6), (3.7), (3.8), (3.16), (3.30), and (3.31), and replacing β in (3.8) by an effective β corrected for gains and losses due to precipitation, resolution and sweeping):

$$\dot{b} = 4\pi D_g nrc - (\eta+f)b$$

$$\dot{c} = \left[\left(\beta - 4\pi D_g nrc+\eta b - (f - K\frac{r}{a})c\right)\frac{a^2}{15D_g} - c\right]\omega(t,\tau) \qquad (3.34)$$

$$f = K\frac{r}{a} + \frac{3S(1-P)}{4a^4} + n_p\sigma_p v_p$$

Since, by definition

$$\int\beta(t)dt = c+b+g$$

the rate of gas release is

$$\dot{g} = \beta - \dot{c} - \dot{b}$$

This has to be divided up into gas going into grain faces, which are adjacent to another grain, and gas released to the porosity. For the gas released via atomic diffusion and intragranular bubble migration, the fraction P is assumed to go directly into the porosity. The gas swept up by pore migration is totally released to the porosity, the gas swept by grain growth is added to the grain face gas. Thus

$$\dot{g}_{gb} = (\dot{g} - (f - K\frac{r}{a})(c+b))(1-P) + \frac{3S(1-P)}{4a^4}(c+b)$$

$$\dot{g}_p = (\dot{g} - (f - K\frac{r}{a})(c+b))P + n_p\sigma_p v_p(c+b) \qquad (3.35)$$

g_{gb} gas released to the grain faces (adjacent to another grain)
g_p gas released to the porosity (fabricated or restructured)

(3.35) links the intragranular equations to those given in the next chapter for the grain faces.

Under transient conditions, different time intervals may be defined with temperatures, production rate and pin internal pressure varying linearly with time. The local hydrostatic pressure is now the result of the calculation of porosity pressurization (see chapter 5). Again, the interval is subdivided and the following set of equations is integrated (see (3.6), (3.7), (3.8), (3.21), (3.23), and (3.33)):

$$\dot{c} = \left[(\beta + (\eta b - 4\pi D_g nrc - cn\pi r^2 v)(1-F)) \frac{a^2}{15 D_g} - c \right] \omega(t,\tau)$$

$$\dot{b} = (4\pi D_g nrc + cn\pi r^2 v - \eta b)(1-F)$$

$$\dot{\tau} = \frac{D_g}{a^2} \qquad (3.36)$$

$$\dot{n} = \frac{16\Omega^{1/3} f(r) n^2 D_s}{\lambda^2 (1+n \frac{4\pi}{3} r^3)} \left(\frac{\pi r^3 Q_s \nabla T_s C_1}{kT^2} + \frac{3\Omega C_2}{r} \right)$$

$$\dot{r} = \dot{r}_{co} + \dot{r}_{pr} + \dot{r}_{c1} + \dot{r}_{c2}$$

In this case, must be integrated numerically, whereas under steady state conditions, i.e. piecewise constant temperatures, an analytic expression can be used. The equation for gas precipitation-resolution is approximately corrected for the effect of partial bubble release by multiplying by 1-F. A swelling correction /15/ is inserted in the coalescence term. Bubble number losses due to resolution are neglected for the short time spans associated with a transient.

For the (1-F)-correction, the F-value at the start of the subinterval is employed. After integrating the system (3.36), the value of F is updated.

The intragranular fission gas driven swelling is calculated from

$$S_1 = n \frac{4\pi}{3} r^3 (1-F) + cL\Omega \qquad (3.37)$$

with F = 0 for the steady state case. Solid fission product swelling is not computed by LAKU.

4. Gas on Grain Faces

The treatment of gas on grain faces is in many ways similar to the one of intragranular gas, since many physical processes are the same. The same notation is used as far as possible with an asterisk denoting grain face quantities.

The geometrical model assumptions used for the grain face gas are based on experimental evidence and are similar to the ones used by other code authors /e.g. 3/. Grain face bubbles are assumed to be lenticular (Fig. 1) with contact angle ψ, uniformly spaced and of equal size. When the fraction B_m of the grain face is covered by bubbles, bubble interlinkage is assumed to occur, venting the bubble gas to the grain edges and the porosity. The bubble radius r* used in the equations is the one associated with the grain surface covered by the bubble and is coupled to the radius of bubble surface curvature (see Fig. 1) by

$$\text{radius of curvature} = \frac{r^*}{\sin\psi} ;$$

the bubble volume is αr^{*3} (see (2.2))

r* radius of grain face bubble

The grain face bubble density n* used in the following equations is a surface density. Assuming that only the fraction 1-P of the grain surface is adjacent to another grain, the grain face bubble density per unit volume is related to the one per unit surface by

$$n^*_{vol} = F_{vol}\, n^* \qquad (4.1)$$

$$F_{vol} = \frac{3}{2a}(1-P)^2$$

n^*_{vol} grain face bubble number density per unit volume
n^* grain face bubble number density per unit surface
F_{vol} ratio of grain face area to volume

The grain is assumed to have 12 neighbours with which it shares a surface. This surface is idealized as a plane circle with radius

$$a^* = a\sqrt{\frac{1-P}{3}} \qquad (4.2)$$

a^* radius of grain face

Using this geometrical picture, the following processes are modeled (compare chapter 3):

A. Formation of grain face bubbles
B. Precipitation of resolved gas into grain face bubbles
C. Resolution of grain face bubble gas
D. Diffusion of resolved gas to the grain edges
E. Migration of grain face bubbles to grain edges
F. Coalescence of migrating bubbles
G. Time dependent bubble volume equilibration. As for intragranular bubbles, this process is treated under transient conditions only, since grain face bubbles are assumed to have equilibrium volume under irradiation conditions.
H. Sweeping processes
I. Gas release by interconnection

In the following equations, the gas components will be denoted as in the intragranular case:

c^*	resolved gas in the grain faces	$[\text{moles/cm}^3]$
b^*	grain face bubble gas	$[\text{moles/cm}^3]$
g^*	gas released from grain faces	$[\text{moles/cm}^3]$

A. Formation and loss of bubbles

Under irradiation conditions, grain face bubbles are assumed to originate from intragranular bubbles released to the grain surface, and to be lost by resolution and migration to the edges. Losses by resolution are reduced, when the bubble radius exceeds the radius of the damage zone of a fission spike, which can be imagined as a long cylinder /23/. Then, the equation describing bubble number gains and losses is

$$\dot{n}^* = -n^*(\eta \cdot \mathrm{Min}(1, \left(\frac{r_f}{r^*}\right)^2) + K^* \frac{r^*}{a} + n^* r^* v^*)$$

$$+ \left(\frac{Kr}{a} + \frac{3S}{4a^4}\right) \frac{1-B}{F_{vol}} n(1-P) \qquad (4.3)$$

r_f radius of damage zone of fission spike
v^* velocity of grain face bubble
B fraction of surface covered by grain face bubbles

In (4.3), the first term describes losses by resolution, release by bubble migration, and coalescence due to bubble migration (see (4.13), (4.15)). The second term contains gains by intragranular bubble migration and by grain boundary sweeping. (4.3) is treated in the same way as the respective equation for intragranular bubbles, i.e. is linearized and solved analytically for a time subinterval; a linear interpolation of the resultant number density at the beginning and end of the subinterval is then used in the integration of the equations for the gas components. The bubble number density is kept constant after interlinkage has been achieved.

In the transient part of the program, the equation for the bubble number density is integrated together with the other equations for grain face gas behaviour. It will be treated in section 4.E.

B. Precipitation

Under stationary conditions, gas is mainly released to the surface via atomic diffusion; of this gas, the fraction B goes directly into the grain face bubbles, whereas the rest diffuses in the face and eventually may reach the bubbles, too. Diffusion is assumed not to lead back into the interior of the grain, since the gas diffusion coefficient of the grain face is much bigger than the intragranular one /24/. Therefore, the geometry used to describe the precipitation process is two-dimensional, with the bubble represented by a flat circle, that is surrounded by a circular cell of its share of grain face area. The solution of the gas diffusion equation for this geometry, with the proper boundary conditions

and taking into account that near bubble interlinkage the cell radius is not much bigger than the bubble radius, is

$$\dot{b}^*_{prec} = 4\pi D^*_g n^* F_B c^*$$

$$F_B = \frac{1-B}{B-1-\ln B} \qquad (4.4)$$

D^*_g grain face diffusion coefficient of atomic gas

C. Resolution

Resolution is described, analogous to (3.7), by

$$\dot{b}^* = -\eta b^* \qquad (4.5)$$

The gas undergoing resolution is added fully to the resolved grain face gas, since the gas atoms are not scattered back very far into the lattice and thus have a high probability of diffusing back to the grain surface. Whereas in (4.3), the bubble number losses due to resolution are reduced for big bubbles, this is not done in (4.5) for the gas contained in such bubbles. The underlying assumption is, that bigger bubbles have a greater probability of being only partly destroyed, whereas the resolution probability for the individual bubble gas atom is independent of bubble volume.

D. Diffusion of atomic gas to grain edges

As in the case of precipitation, this process is treated analogous to the intragranular case in two-dimensional circular geometry (see (3.8), (3.9)):

$$c^*_{as} = \beta^*(t)\,\frac{a^{*2}(t)}{8D^*_g(t)}$$

$$\frac{dc^*(t)}{dt} = \omega^*(t,\tau^*)\left(\frac{\beta^*(t)a^{*2}(t)}{8D^*_g(t)} - c^*(t)\right) \qquad (4.6)$$

$$\frac{d\tau^*(t)}{dt} = \frac{D^*_g(t)}{a^{*2}(t)} \qquad (4.7)$$

$$\omega^*(t,\tau^*) = \frac{D^*(t)}{\frac{g}{a^{*2}(t)}} \left(\sum_{i=1}^{\infty} \frac{1}{x_i^2} \exp(-x_i^2 \tau^*) \right) \left(\sum_{i=1}^{\infty} \frac{1}{x_i^4} \exp(-x_i^2 \tau^*) \right)^{-1}$$

β^* effective grain face gas source term

x_i zeros of zero'th order Bessel functions

Again as in the intragranular case, τ^* is integrated continuously, but may be reset to zero, if temperatures are considerably reduced during irradiation.

E. Bubble migration

Contrary to intragranular bubble migration, this process is not very important for both stationary and transient grain face gas release, since release by interconnection or atomic diffusion is more effective under most conditions. Nevertheless, it has to be modeled, since grain face bubble overpressure is influenced by it, and this is an important parameter for fuel failure criteria.

The bubble diffusion coefficient due to surface diffusion is, for lenticular bubbles /15,1/:

$$D_b^* = \frac{4\pi\Omega^{4/3} D_s}{(1+\cos\psi)\alpha^2 r^{*4}} \tag{4.8}$$

D_b^* diffusion coefficient of grain face bubbles

Here, the bubbles are assumed to be much bigger than the mean jump distance of surface atoms, which was accounted for in the corresponding intragranular equations (3.10). For a mean angle of $\pi/4$ between temperature gradient and grain surface, the bubble velocity is

$$v^* = \frac{\alpha r^{*3}}{\Omega} \frac{Q_s \nabla T_s D_b \sin\pi/4}{kT^2} = \frac{4\pi\Omega^{1/3} Q_s \nabla T_s D_s \sin\pi/4}{(1+\cos\psi)\alpha r^* kT^2} \tag{4.9}$$

The fraction of bubbles removed to the grain edges by biased migration is given by a formula corresponding to (3.13) for two-dimensional geometry /1/:

$$F^*(s^*) = \frac{2}{\pi}\left(\arcsin\frac{s^*}{2a^*} + \frac{s^*}{2a^*}\sqrt{1 - \frac{s^{*2}}{4a^{*2}}}\right) \qquad s \leq 2a^*$$

$$= 1 \qquad s > 2a^* \qquad (4.10)$$

F^* fraction of bubbles released to grain edges

s^* migration distance of grain face bubbles,

$$s^* = \int_0^t v^*(t')dt'$$

(4.10) would be sufficient, if the surface area voided by migration were not replenished by bubbles released from the interior of the grain. Thus, an approximately uniform distribution of bubbles is kept up a long time during the release process. Therefore, instead of using the cumulative F^* from (4.10), a correction containing

$$\Delta F^* = F^*(\Delta s^*) \qquad (4.11)$$

$$\Delta s^* = \int_0^{\Delta t} v^*(t')dt'$$

is applied to b^* and g^* after each time interval of a transient. The error introduced by this approximation, which always employs the initial value of F^*, is not very big, since most gas release from grain face bubbles is by bubble interconnection. The technique used for the transient is thus as follows: The differential equations for the grain face gas are formulated excluding release by migration, but including coalescence and sweeping caused by migration, and solved first for Δt. Then, the following correction is applied to the results:

$$n^*_{korr} = n^* \ (1-\Delta F^*)$$

$$b^*_{korr} = b^* \ (1-\Delta F^*) \qquad (4.12)$$

$$g^*_{korr} = g^*+b^*\Delta F^*$$

Conditions are similar for steady state simulation; therefore the initial value of the differential release fraction is employed as in the intragranular case (see (3.16)):

$$\frac{dF^*}{dt} \simeq \left.\frac{dF^*}{ds^*}\right|_{s^*=0} v^* = \frac{2v^*}{\pi a^*}$$

$$\left(\frac{\dot{b}^*}{b^*}\right)_{migr} = \left(\frac{\dot{n}^*}{n^*}\right)_{migr} = -K^* \frac{r^*}{a} \qquad (4.13)$$

$$K^* = \frac{2\alpha}{\pi} \frac{Q_s \nabla T_s D_{b0} \sin\pi/4}{\Omega k T^2} \sqrt{\frac{3}{1-P}}$$

F. Bubble coalescence

Coalescence is calculated in the same way as for intragranular bubbles, taking into account the plane geometry. Instead of (3.17), the number of coalescences in a time interval Δt for two classes of bubbles with radii r_1^*, r_2^*, velocities v_1^*, v_2^*, and number densities n_1^*, n_2^* is now given by

$$G^*_{12} = n^*_1 \ n^*_2 \ (2r^*_1 + 2r^*_2) \ |v^*_1 - v^*_2| \ \Delta t \qquad (4.14)$$

This is approximated, for one bubble group, by

$$\dot{n}^*_{co} = - \frac{n^{*2}}{2} 4r^*v^*C_3 \qquad (4.15)$$

with the correction factor C_3 accounting for the effect of the actual size distribution. $C_3 = 0,5$ is currently used /17,1/. (4.15) turns up in the transient equations for the bubble number density as well as in the equation for steady state bubble number growth (4.3).

G. Bubble volume equilibration

Under irradiation conditions, grain face bubbles are assumed to have their equilibrium volume. In transients, there are five contributions to the change of bubble volume

$$\dot{r}^* = \dot{r}^*_{co} + \dot{r}^*_{pr} + \dot{r}^*_{re} + \dot{r}^*_{c1} + \dot{r}^*_{c2} + \dot{r}^*_{c3} \tag{4.16}$$

which are due to, respectively: Coalescence, precipitation of atomic gas, release of intragranular bubbles, and three creep processes. The first term is given by (see (3.24)):

$$\dot{r}^*_{co} = -\frac{r^*}{3}\frac{\dot{n}^*_{co}}{n^*} \tag{4.17}$$

For the second and third term, the treatment of intragranular bubbles arriving on the grain face must be presented first. Of course, a fraction of the released bubbles coalesces directly with the grain face bubbles. The program chooses between two options for the treatment of the rest:

Option 1: If the grain face bubble volume is more than a factor 8 bigger than the volume of the released bubbles, the gas content of the released bubbles is added to the resolved grain face gas.

Option 2: Otherwise, the two bubble populations are averaged.

Possibly, an explicit treatment of the two populations should be realized in the long run.

If the first option is used, the volume associated with the released intragranular bubbles would be lost, if it was not explicitly accounted for. Therefore, instead of attributing one vacancy to each resolved gas atom a "virtual" volume is assigned to it. At the start of the transient

$$\Omega_{vir}(0) = \Omega \tag{4.18}$$

Ω_{vir} virtual volume assigned to gas atom resolved in grain surface during transient

The virtual volume is updated for each time step Δt in the following way:

Total amount of gas released from the grain in Δt, by atomic diffusion and gas bubble migration:

$$g_{tot} = g(t+\Delta t)-g(t)+b(t+\Delta t)F(t+\Delta t)-b(t)F(t) \tag{4.19}$$

Mean number of gas atoms contained in the released bubbles:

$$n_a = \frac{L}{2}\,(b(t+\Delta t)/n(t+\Delta t) - b(t)/n(t)) \tag{4.20}$$

Mean volume per gas atom released to the grain face:

$$\bar{V} = \frac{4\pi}{3n_a g_{tot}}\left(\frac{3\Omega n_a}{4\pi}\,(g(t+\Delta t)-g(t) + \frac{1}{2}\,(r^3(t+\Delta t)+r^3(t))(b(t+\Delta t)F(t+\Delta t)-b(t)F(t))\right) \tag{4.21}$$

Updated value of Ω_{vir}:

$$\Omega_{vir}(t+\Delta t) = (c^*(t)\Omega_{vir}(t) + \frac{1}{2}\,(\eta(t)+\eta(t+\Delta t))b^*(t)\Delta t\Omega + g_{tot}(1-B^*)\delta(\emptyset)\bar{V})/(c^*(t) + \frac{1}{2}\,(\eta(t)+\eta(t+\Delta t))b^*(t)\Delta t + g_{tot}(1-B^*)\delta(\emptyset))^{-1} \tag{4.22}$$

$$B^* = n^*\,(r^*+\bar{r})^2$$

$$\bar{r} = \sqrt[3]{\bar{V}\,\frac{4\Omega}{3\alpha}}$$

$\delta(\emptyset) = 1$ for option 1

0 for option 2

The term containing η accounts for the gas redissolved in Δt. Ω_{vir} is always updated before the differential equations for grain face gas are solved for the time interval Δt. With the actual value of Ω_{vir}:

$$\dot{r}^*_{pr} = (4\pi D^* n^* F_B c^* + 2c^* n^* r^* v^*) \frac{\Omega_{vir} L}{3\alpha F_{vol} n^* r^{*2}} \tag{4.23}$$

The effect of bubble sweeping (see 4.H) is included in (4.23).

The third term in (4.16) is

$$\dot{r}^*_{re} = \frac{V(1+(B^*-1)\delta(\phi))}{3\alpha n^* r^{*2}} \cdot \frac{g_{tot}(1-P)L}{\Delta t \; F_{vol}} \tag{4.23}$$

Creep processes are again subdivided into creep caused by vacancy diffusion ($\dot{r}^*_{c1} + \dot{r}^*_{c2}$) and high temperature dislocation climb and glide ($\dot{r}^*_{c3}$). The first term is modeled explicitly; intragranular and grain face vacancy diffusion are separated. The grain face vacancy diffusion is given by /25/

$$\dot{r}^*_{c1} = \frac{D^*_u \delta^* \Omega 4\pi p^*_{ex} F_B}{3\alpha r^{*2} kT} \tag{4.24}$$

D^*_u self diffusion coefficient of heavy species in grain face

δ^* width of grain face

p^*_x excess pressure in grain face bubble

The contribution of intragranular vacancies is calculated approximately in plane geometry, assuming that vacancies flow to the surface of the grain face bubble from the interior of the grain only from half the mean distance to the next intragranular bubble. From geometric considerations, the mean distance 2X can be estimated as

$$2X = \frac{4a}{3+aS_1/r} \tag{4.25}$$

Using the same kind of analysis as Greenwood et al. /18/ for plane geometry, one arrives at

$$\dot{r}^*_{c2} = \frac{4\pi}{3\alpha}\frac{D_u}{X}\frac{p^*_{ex}}{1+\cos\psi}\frac{\Omega}{kT} \qquad (4.26)$$

High temperature creep is modeled analagous to the intragranular case. The ratio of total volume to total grain face bubble volume is

$$\frac{1+S_1}{\alpha r^{*3} n^* F_{vol}} + 1 \simeq \overline{(r^*_z/r^*)}^3$$

Then, similar to (3.28)

$$\dot{r}^*_{c3} = r^* \frac{C}{2} \exp(-H/kT) \left[\frac{\frac{3}{2m} p^*_{ex}}{\overline{(r^*_z/r^*)}^{3/m} - 1}\right]^m \qquad (4.27)$$

H. Sweeping processes

Only sweeping of resolved gas by the migrating grain face bubbles must be modeled, and its effect is small. Under irradiation conditions, bubbles are either small and immobile - at low temperatures - or the resolved gas concentration is negligible because of the enhanced atomic gas diffuison in grain faces - at high temperatures. For transient conditions, if the fuel is heated very rapidly, the bubbles may become mobile before all gas has been precipitated. For these reasons, the effect is modeled only in the transient part. The contribution is

$$\dot{b}^*_{bs} = 2r^* v^* n^* c^*$$

$$= \frac{8\pi\Omega^{1/3} Q_s \nabla T_s D_s \sin\pi/4}{(1+\cos\psi)\alpha k T^2} n^* c^* \qquad (4.28)$$

I. Interconnection

It is assumed to take place when the area covered by grain face bubbles exceeds a critical value B_{max}. Under irradiation conditions, the number of

bubbles and their radius are kept constant after reaching this condition, i.e. all gas arriving at the face after interconnection is directly transferred to the edges. In the transient part, bubbles are allowed to continue growing, and the number of bubbles is reduced to conserve B_{max}, i.e. bubbles are transferred to the edges:

$$n^*_{korr} = \frac{B_{max}}{\pi r^{*2}}$$

$$b^*_{korr} = b^* \frac{B_{max}}{\pi n^* r^{*2}} \qquad (4.29)$$

$$g^*_{korr} = g^* + b^* \left(1 - \frac{B_{max}}{\pi n^* r^{*2}} \right)$$

B_{max} maximum fraction of surface covered by grain face bubbles

This correction is applied after calculating losses due to migration (see (4.12)).

The equations for grain face gas will now be summarized separately for the steady state and transient part. In both parts, the same time subintervals are used for the evaluation of the intragranular and grain face gas equations; the changes of all gas components are calculated for one subinterval before proceeding to the next. This is done in the steady state part by directly integrating all equations together; in the transient part, the intragranular equations are integrated first, then the release from the interior of the grain is evaluated and fed as a source term to the grain face equations, which are integrated separately.

The steady state part starts with the evaluation of the changing grain face bubble number by using an analytic approximation to the solution of (4.3). The result is linearized for the subinterval and used for the numerical integration of the steady state grain face gas equations (see (4.4), (4.5), (4.6), and (4.13)):

$$\dot{b}^* = \dot{g}_{gb}B + 4\pi D_g^* n^* F_B c^* - (\eta + f^*)b^*$$

$$\dot{c}^* = \left[(\dot{g}_{gb}(1-B) - 4\pi D_g^* n^* F_B c^* + \eta b^*) \frac{a^{*2}}{8D_g^*} - c^* \right] \omega^*(t,\tau^*)$$

$$f^* = K^* \frac{r^*}{a} \tag{4.30}$$

The transient part for the grain face gas starts with the evaluation of the source terms and related quantities, eq.s (4.19) - (4.22), and, for subinterval length Δt

$$q_g = g_{tot}(1-P)/\Delta t$$

$$q_n = q_g L/(n_a F_{vol}) \tag{4.31}$$

q_g transient rate of gas arriving at grain face
q_n transient rate of bubbles arriving at grain face (per unit area)

The choice is made between option 1 and 2 for treatment of the released intragranular bubbles. The equations to be integrated are then (see (4.4) - (4.7), (4.15), (4.16), and (4.28)):

$$\dot{c}^* = \left[(q_g(1-B^*)\delta(\emptyset) + \eta b^* - 4\pi D^* n^* F_\beta c^* - 2r^* v^* n^* c^*) \frac{a^{*2}}{8D_g^*} - c^* \right] \omega^*(t,\tau^*)$$

$$\dot{b}^* = 4\pi D^* n^* F_B c^* + 2r^* v^* n^* c^* + q_g(1+(B^*-1)\delta(\emptyset)) - \eta b^*$$

$$\dot{\tau}^* = \frac{D_g^*}{a^{*2}} \tag{4.32}$$

$$\dot{n}^* = q_n(1-B^*)(1-\delta(\emptyset)) - K^* \frac{r^*}{a}$$

$$\dot{r}^* = \dot{r}_{co}^* + \dot{r}_{pr}^* + \dot{r}_{re}^* + \dot{r}_{c1}^* + \dot{r}_{c2}^* + \dot{r}_{c3}^*$$

As in the intragranular case, τ^* must be integrated numerically in the transient part only, and bubble number losses due to resolution are neglected.

The contribution of grain face gas to fission gas driven swelling is given by

$$S_2 = n^*_{vol}\ \alpha r^{*3} + c^* L \Omega_{vir} \qquad (4.33)$$

5. Gas in Porosity

The gas released from the grain faces goes to the grain edges - a small fraction of it goes directly into the fabricated porosity -, where it eventually forms tunnels interlinking the porosity and leading to the release of porosity and grain edge gas to ambient. In principle, the formation and interlinkage of grain edge bubbles could be treated with a model similar to the intragranular and grain face models. This possibility was rejected as too cumbersome for the small amount of gas involved. Instead, a simple model was devised for treating the growth of the fabricated porosity and the formation of interlinking tunnels together. Its few parameters are chosen to fit results to existing measurements.

The model assumes that there is one fabricated pore per fuel grain, which is idealized as a sphere. The initial number of pores and their initial radius are determined by as fabricated fuel porosity and grain radius:

$$n_p(0) = \frac{1-P}{\frac{4\pi}{3} a_o^3}$$

$$r^{**}_{eff}(0) = a_o \sqrt[3]{\frac{P}{1-P}} \qquad (5.1)$$

n_p number density of pores

r^{**}_{eff} effective pore radius (including tunnel volume) of closed pores

The pores are assumed to contain, initially, fill gas at room temperature and pressure, the amount of which is determined from the equation of state (2.1) or (2.3). Depending on the porosity of the fresh fuel, a fraction of the fabricated pores may already be "open", i.e. be linked to the ambient by a network of tunnels. During irradiation or a transient, the remaining "closed" pores will gradually transform into open ones due to the formation of additional tunnel length. The tunnels are assumed to be cylindrical with a cone-like opening into the pore and a cone-shaped tip (see Fig. 3). For fresh fuel, rudimentary tunnels are assumed to sit on the surface of the pore. Six tunnels are assumed to originate from each pore and to occupy, at the beginning, the fraction ε of the effective pore volume given by $r^{**}_{eff}(0)$. The radius of the pore without tunnels is

$$r^{**}(0) = r^{**}_{eff}(0) \sqrt[3]{1-\varepsilon} \tag{5.2}$$

r^{**} radius of closed pore (without tunnels)

ε fraction of pore volume in unirradiated fuel going into tunnel formation

Time dependent pore and tunnel growth is caused by creep and by the volume associated with released intragranular and grain boundary gas and gas bubbles. The treatment of growth is somewhat different in the steady state or transient case, since restructuring has to be taken into account during irradiation; creep is treated in both cases, but omitting the high temperature component in the steady state case. Only the open pores are assumed to be affected by restructuring, and only the closed ones by creep.

The growth of closed porosity is presented first. With released gas and the associated volume being equally divided among the closed and open pores

$$r^{**3}_{eff}(t+\Delta t) = r^{**3}_{eff}(t) + \frac{\delta V}{n_p(t)\,\frac{4\pi}{3}} \tag{5.3}$$

δV volume associated with gas released in time step Δt to grain edges and pores - per cubic cm of fuel

δV goes mainly into tunnel formation, since most gas release is to the edges and not directly into the pores; only a fraction corresponding to the porosity of the closed pores

$$F_p = n_p(t)\,\frac{4\pi}{3}\,r^{**3}(t)$$

is added to the pore volume:

$$r^{**}(t+\Delta t) = r^{**}(t) \sqrt[3]{1+\delta V} \tag{5.4}$$

Contrary to intragranular and grain faces bubbles, which under stationary conditions are assumed to have their equilibrium volume, the growth of closed porosity due to creep is treated explicitly for steady state as well as transient conditions; this is due to the bigger dimensions of the

pores, which result in lower excess pressures and thus bigger time constants for growth. Creep due to vacancy migration in grain faces and in the interior of the grain is treated using a weighted uranium self diffusion coefficient

$$w \simeq \frac{3}{2}\frac{\delta}{r^{**}(t)}$$

$$D_u^{eff} = wD_u^* + (1-w)D_u \tag{5.5}$$

with the weight factor w derived from geometric considerations for pores and tunnels. The growth of the effective pore radius in time interval Δt is then approximated by (see (3.26)):

$$\Delta r^{**}_{eff,c1} = \frac{D_u^{eff}\,\Omega p^{**}_{ex}}{r^{**}_{eff}\,kT}\,\Delta t \tag{5.6}$$

p^{**}_{ex} excess pressure in closed pore

In the transient part, the effect of high temperature creep is added (see (3.28)):

$$\Delta r^{**}_{eff,c2} = r^{**}_{eff}\,\frac{C}{2}\exp(-H/kT)\left[\frac{\frac{3}{2m}\,p^{**}_{ex}}{(r^{**}_z/r^{**}_{eff})^{3/m}-1}\right]^m \Delta t \tag{5.7}$$

$2r^{**}_z$ mean distance between two closed pores

The growth of the effective pore radius due to creep is thus

$$\Delta r^{**}_{eff} = \Delta r^{**}_{eff,c1} + \Delta r^{**}_{eff,c2}$$

$$r^{**}_{eff}(t+\Delta t) = r^{**}_{eff}(t) + \Delta r^{**}_{eff} \tag{5.8}$$

and assuming that the relative volume increase is the same for pore and tunnels:

$$r^{**}(t+\Delta t) = r^{**}(t)(1+\Delta r^{**}_{eff}/r^{**}_{eff}) \tag{5.9}$$

From r^{**}_{eff} and r^{**}, the volume of each of the six tunnels starting at the pore results as

$$\Delta V = \frac{2\pi}{9} (r^{**3}_{eff} - r^{**3})$$

and from ΔV and the geometry assumed for the tunnel (Fig. 3), the length of the tunnel is calculated as

$$x_c = \sqrt[3]{3\Delta V/(\pi \cdot tg^2\psi)}$$

$$\text{if } x_c < x_c^c = r^{**} \frac{1-\sin\psi}{\sin\psi}$$

$$x_c = x_c^c + (\Delta V - (x_c^c)^3 \frac{\pi \cdot tg^2\psi}{3}) / \pi r_c^2 \qquad (5.10)$$

otherwise

x_c length of tunnel attached to closed pore

r_c radius of tunnel attached to closed pore,

$$r_c = \text{Min}(r^{**}/5,\ .75 \cdot 10^{-5} \text{cm})$$

Next, the treatment of the open pores is presented. Under steady state conditions, they are assumed to be affected by restructuring. With one pore per (growing) grain, including the closed pores, the time dependent number of open pores is

$$n_p^{\emptyset}(t) = \frac{1-P(t)}{\frac{4\pi}{3} a^3(t)} - n_p^c(t) = n_p(t) - n_p^c(t)$$

(if, as may happen early on during restructuring, $n_p^c(t) > n_p(t)$, more than one pore per grain are admitted; then, $n_p^{\emptyset}(t) = 0$, $n_p(t) = n_p^c(t)$)

n_p^c number density of closed pores

$n_p^{\emptyset}$ number density of open pores

and their effective radius is given by the time dependent porosity

$$r_p^{**}(t) = \sqrt[3]{\frac{P(t)}{\frac{4\pi}{3} n_p(t)}} \qquad (5.11)$$

r_p^{**} effective radius of open pores

(5.11) ensures that fission gas driven swelling caused by the pores goes to zero when all pores are open under steady state conditions.

No steady state creep driven by excess pressure occurs for the open pores, since they can vent. The gas volume released to them during irradiation is assumed to be lost to restructuring, and thus is not accounted for in (5.11), but its effect in elongating the tunnels attached to the open pores is taken into account. The tunnel length of the first pores to open is

$$x_\phi = x_c$$

x_ϕ length of tunnels attached to open pores

The elongation of these tunnels in time step Δt is

$$\Delta x_\phi = \frac{\delta V}{6\pi n_p^\phi r_\phi^2} - v_p \Delta t/3 \qquad (5.12)$$

r_ϕ radius of tunnel attached to open pore,

$$r_\phi = \text{Min}(r_p^{**}/5, 7.5\text{-}5\text{cm})$$

The last term in (5.12) accounts for the shortening of tunnels caused by pore migration.

Restructuring is omitted in the transient part, and therefore the open porosity may swell and tunnels grow faster. Creep due to excess pressure is neglected, since the pressures built-up due to noninstantaneous gas release from the open porosity are generally low. With these approximations, the growth of the effective radius of open pores and of their tunnels during transients is given by

$$r_p^{**3}(t+\Delta t) = r_p^{**3}(t) + \frac{\delta V}{\frac{4\pi}{3} n_p^{\phi}} \tag{5.13}$$

$$\Delta x_{\phi} = \frac{\delta V}{6\pi r_{\phi}^2 n_p^{\phi}} \tag{5.14}$$

The average tunnel length for closed and open pores is then

$$\bar{x} = (x_c n_p^c + x_{\phi} n_p^{\phi})/(n_p^c + n_p^{\phi}) \tag{5.15}$$

$\bar{x}$ average tunnel length

These tunnels stretch along the edges of the grain faces. The total length of the edges per pore is, for the geometry with 12 grain faces used in the foregoing chapter

$$X_t = 12\pi a\left(\frac{1-P}{3}\right)^{3/2}$$

with the fraction 1-P of the edges assumed to border directly on pores. Of this length, the fraction F_t is covered by tunnels:

$$F_t = \frac{6\bar{x}}{X_t} = \frac{\bar{x}}{2\pi a}\left(\frac{3}{1-P}\right)^{3/2}$$

Every two tunnels from neighbouring pores make up one channel linking the pores. Among the six channels originating from one pore, three must be considered as ingoing and three as outgoing links. The number of open outgoing links is assumed to be

$$L_p = 3F_t = \frac{3\bar{x}}{2\ a}\left(\frac{3}{1-P}\right)^{3/2} \tag{5.16}$$

L_p average number of links per pore

Similar to other approaches to the release problem /3,9/ the results of percolation analysis are now used to derive the fraction of open pores from L_p. According to Maschke et al. /16/, all pores are interlinked, when L_p reaches the value 1.569. In reality, interlinkage will occur gradually when L_p approaches and exceeds this critical value, due to the statistical

variations of the material parameters. The interlinkage fraction is therefore given by the following integral /9/

$$F_p = \frac{1}{\sqrt{2\pi}\sigma} \int_{1.569}^{\infty} \exp(-(u-L_p)^2/2\sigma^2)du \qquad (5.17)$$

F_p fraction of open pores

where the variation σ of L_p can be evaluated from experimental histograms of pore and grain size and fractional porosity. Since $\bar{x}$ depends on these parameters in a very complicated way, a simplified approach is taken. Neglecting the smaller influence of pore size and porosity distribution, and the variation in x, (5.16) leads to

$$\sigma = \sigma_a L_p$$

σ_a relative variation of grain size

as a first estimate for σ. This formula leads to a broadening distribution for growing L_p, which is not quite realistic, since for L_p approaching the limiting value of 3 (i.e. all channels open), the distribution should narrow. To achieve this, the modified formula

$$\sigma = \sigma_a L_p(1-L_p/3) \qquad (5.18)$$

is used, which ensures a total opening of pores at maximum tunnel length.

From F_p, the number of open pores results as

$$n^{\emptyset}(t) = n_p(t)F_p(t) = \frac{1-P(t)}{\frac{4\pi}{3}a^3(t)} F_p(t) \qquad (5.19)$$

For a given number of pores opening in time step Δt, the average tunnel length of open pores must be corrected:

$$n_p^{\emptyset} = n_p^{\emptyset}(t+\Delta t) - n_p^{\emptyset}(t) \qquad (5.20)$$

$$x_{\emptyset}^{corr}(t+\Delta t) = (x_{\emptyset}(t+\Delta t)n_{\emptyset}(t) + x_c(t+\Delta t)\Delta n_p^{\emptyset})/n_p^{\emptyset}(t+\Delta t)$$

For the transient part, the effective radius of the open pores must be adjusted, too:

$$(r_p^{**corr}(t+\Delta t))^3 = ((r_p^{**}(t+\Delta t))^3 n_\phi(t) + r_{eff}^{**}(t+\Delta t))^3 \Delta n_p^\phi) / n_p^\phi(t+\Delta t) \qquad (5.21)$$

The quantity of gas residing in closed and open pores and released to ambient is

$$g_c = n_p^c(t) \cdot \nu_p$$

$$g_\phi = \text{Min}(n_p^\phi(t) \nu_g(T,p,r_p^{**}), g_p + g^* - g_c) \qquad (5.22)$$

$$g_r = g_p + g^* - g_c - g_\phi$$

g_c gas in closed porosity
g_ϕ gas in open porosity
g_r gas released to ambient
ν_p gas released to one pore
ν_g gas content of one open pore, as determined by equation of state

Swelling due to pore expansion is given by

$$S_3 = \frac{4\pi}{3} (n_p^c r_{eff}^{**3} + n_p^\phi r_p^{**3}) - P \qquad (5.23)$$

S_3 porosity swelling

The gas in the open pores is free to vent to the central cavity, the fuel-cladding gap and the fission gas plenum. This process is assumed to be instantaneous under irradiation conditions, with only a small fraction of gas determined by the equation of state and the effective radius of the open pores remaining in the fuel. This is also the starting condition for transients except experiments, which entail cooling and cutting of the fuel; for this case, the open pores are assumed to be totally vented and refilled with fill gas at the starting conditions of the experiment.

Gas release from the open pores cannot be expected to be instantaneous for all transient conditions, especially for short duration transients and/or

low fuel permeability. A model for calculating the resulting pressure buildup in the open porosity has been devised by Hofmann and Meek /19/. Their formalism was extended to accommodate the surface tension in the pores and a non-equidistant mesh, and then coupled to LAKU. Its main restriction is, at present, the assumption of an intact fuel pellet, excluding the treatment of cracked fuel.

Assuming circumferential symmetry, neglecting axial gradients, and with some further simplifications as specified by Hofmann and Meek, the equations for the conservation of mass and momentum are

$$p \frac{\partial \rho}{\partial t} + \frac{1}{x} \frac{\partial}{\partial x} (\rho x u) = Q'$$

$$- \frac{\kappa}{\mu} \frac{\partial p}{\partial r} = u \qquad (5.24)$$

ρ density of gas in open pores
x radial coordinate
u superficial (Darcy) velocity
Q' source of gas released to pores $[g/cm^3 s]$
κ permeability
μ viscosity of inert gas

By combining these two equations and using the simplified equation of state

$$p + \frac{2\gamma}{r_p^{**}} = \rho \frac{R}{A} T$$

A atomic weight of gas $[g/mole]$

one can eliminate ρ and u to arrive at a single equation for the space dependent gas pressure in the open pores:

$$\frac{\partial p}{\partial t} = - \frac{\partial}{\partial t} \left(\frac{2\gamma}{r_p^{**}} \right) + \frac{p+2\gamma/r_p^{**}}{T} \frac{\partial T}{\partial t} + \frac{RTQ}{\varepsilon} + \frac{T}{\varepsilon r} \frac{\partial}{\partial r} \left(\frac{r\kappa(p+2\gamma/r_p^{**})}{\mu T} \frac{\partial p}{\partial r} \right) \qquad (5.25)$$

Q source of gas released to pores [moles/cm³s]

The boundary conditions are

- outer boundary r_a

  - cladding intact and in contact with fuel:

$$\left.\frac{\partial p}{\partial r}\right|_{r=r_a} = 0 \qquad (5.26a)$$

  - otherwise:

$$p(t,r_a) = p_a(t) \qquad (5.26b)$$

p_a gas pressure in gap

- inner boundary r_i

  - without central void ($r_i = 0$)

$$\left.\frac{\partial p}{\partial r}\right|_{r=0} = 0 \qquad (5.26c)$$

  - with central void

$$p(t,r_i) = p_i(t) \qquad (5.26d)$$

p_i gas pressure in central void

p_a is input, whereas p_i is calculated internally from the quantity of gas flowing to the central void and the temperature of the fuel around the void. No axial effects on p_i are taken into account, since the LAKU model is for one cross section of a pin only; on the other hand, p_i never reaches the very high values by which LAKU-results would be significantly influenced.

Initial conditions are

$$p(r,0) = p_a(0) \qquad (5.27)$$

The numerical procedure used to solve (5.25) - (5.27) is the one of Hofmann and Meek, i.e. the equations are discretized in space and time and integrated with a method that can be varied between explicit and fully implicit. It was found that a semi-implicit procedure worked well. A maximum spatial step length is employed, which often is smaller than some of the radial zones used for calculating the evolution of intragranular and grain boundary gas. Therefore, a finer spatial mesh is used for this part of the program; this mesh is automatically determined at the start of a transient. Averaged pressures are transferred to the coarser mesh of the other program parts. Time step lengths are decoupled for both program parts, too. For a given "macro" step, first all equations save the ones for pressure buildup in the open pores are solved using suitable "micro" time steps, and with an extrapolated value for pore pressures. This results in the time dependent source of gas released to the open pores, which is fed to the pressure buildup part. This part then solves for the same macro step, using its own optimum micro step lengths. If necessary, an iteration is carried out between the two program parts to achieve convergence on the pressures.

6. Modeling Elongated Grains

For simplicity, all formulas in chapters 3 - 5 are given for spherical grains but, as was stated in the introduction already, the formation of elongated grains in the hotter parts of the pin is taken into account. It was decided to model this effect, when difficulties were encountered trying to fit the code parameters to measured gas release data in the temperature range around 1500°C. The introduction of the model successfully relieved these difficulties. Since gas retention at higher temperatures is fairly low, some approximations in deriving the formulas are in order.

The fabricated grain is, as before, idealized as a sphere, but now growth in the radial direction is assumed to be more pronounced than in the other two directions. The geometric representation of this effect is achieved by splitting the grain in two half-spheres and inserting a cylinder (Fig. 4). Growth in the axial and azimuthal direction is assumed to be half of what it would be for spherical growth; growth in the radial direction is augmented, using the condition that the resulting grain volume is identical to the one for spherical growth. The radius of the two half-spheres and the height of the inserted cylinder result from this as

$$a_e = \frac{a_o + a}{2}$$

$$h = \frac{4}{3} a_e ((a/a_e)^3 - 1) \qquad (6.1)$$

The ratio of the long and short grain axes is, for very large grains ($a_e >> a_o$)

$$a_e : a_e + h/2 = 1 : 17/3$$

This is representative of the geometry observed in the hotter zones of pins (e.g. /8/).

Due to the condition for growth, the grain volume remains unchanged, but the grain surface is augmented:

$$V = \frac{4\pi}{3} a^3$$

$$O = \frac{4\pi}{3} a_e^2 (1+2(a/a_e)^3) \qquad (6.2)$$

For large grains, the augmentation is a little less than 50 %.

The geometry of the grain faces has to be changed as well to accommodate the new model. Among the 12 faces 6 are assumed to remain circular - those situated at the ends of the elongated grain - with a radius given by (see (4.2)):

$$a_e^* = a_e \sqrt{\frac{1-P}{3}} \qquad (6.3a)$$

The other 6 are assumed to occupy the length of the grain and are represented by half-circles with rectangles of height h* inserted in-between. h* results from (6.2) and (6.3a), assuming the fraction 1-P of the surface is pore surface:

$$h^* = \frac{2\pi}{3} a_e^* ((a/a_e)^3 - 1) \qquad (6.3b)$$

The change in grain geometry entails the following changes in formulas:

A. Intragranular gas

Here all formulas describing diffusion and migration out of the grain are to be altered. For diffusion processes, $1/a^2$ has to be replaced by an effective value, that is approximately calculated as the mean value of $1/a^2$ for the three different axes. Thus, $1/a^2$ in (3.8), (3.9), (3.34), and (3.36) is to be replaced by

$$\overline{1/a^2} = \frac{2}{3a_e^2} + \frac{3}{a_e^2(1+2(a/a_e)^3)^2} \qquad (6.4)$$

The temperature gradient and thus the biased migration of intragranular gas bubbles is assumed to be in the direction of the long axis of the grain. Employing a picture similar to Fig. 2 for the elongated grain, one arrives at the following formula replacing (3.13) for bubble release during transients:

$$F_b = \frac{3}{4}\frac{a_e s}{a^3} \qquad s \leq h$$

$$F_b = \frac{a^3 - a_e^3 + \frac{s-h}{4}\left(3a_e^2 - \frac{(s-h)^2}{4}\right)}{a^3} \qquad h \leq s \leq h+2a_e \qquad (6.5)$$

$$F_b = 1 \qquad s \geq h+2a_e$$

From (6.5), the effect of bubble migration under irradiation conditions is deduced as

$$\left(\frac{\dot{n}}{n}\right)_{migr} = \left(\frac{\dot{b}}{b}\right)_{migr} = -K\frac{r a_e^2}{a^3} \qquad (6.6)$$

(6.6) must replace (3.16) and be inserted instead of Kr/a in (3.34) - (3.36) and (4.3).

Since the grain volume is unaffected by the change in geometry, the grain boundary sweeping terms which depend on volumetric changes remain unaltered.

B. Gas on grain faces

As the surface to volume ratio is different for spherical and elongated grains, the factor relating grain face bubble densities per unit volume and unit area, F_{vol} from (4.1), is to be replaced by (see (6.2))

$$F_{vol} = (1-P)^2 \frac{1}{a_e}\left(1 + \frac{1}{2}(a_e/a)^3\right) \qquad (6.7)$$

Again $1/a^{*2}$ occurring in the formulas for atomic gas diffusion out of the grain face areas has to be replaced by a suitably averaged value. By assuming the resolved gas to have the same density on small and big grain faces - which is not quite correct, but does not introduce a big error, since the gas component involved is small, - one has

$$\overline{1/a^{*2}} = \frac{1}{4a_e^{*2}(1+2(a/a_e)^3)} \left[6+(4(a/a_e)^3-1)* \right.$$

$$\left. *\left(1 + \frac{1}{(1+\frac{\pi}{3}((a/a_e)^3-1))^2}\right)\right] \qquad (6.8)$$

(6.8) is to be inserted in (4.6), (4.7), (4.30), and (4.32).

For treatment of intergranular bubble migration, a constant bubble density on all surface areas is assumed. The bubble velocity on the small surface areas is assumed to be half the one on the big areas, which are parallel to the temperature gradient. Then $\sin\pi/4$ has to be replaced by

$$\sin\pi/4 \leftarrow \frac{8(a/a_e)^3+1}{4(2(a/a_e)^3+1)} \qquad (6.9)$$

in (4.9) and (4.28).

The fraction of bubbles released to the grain edges by bubble migration is calculated separately for small and large surface areas and then weighted:

$$F_s^* = \frac{2}{\pi}\left(\arcsin\frac{s^*}{4a_e^*} + \frac{s^*}{4a_e^*}\sqrt{1-\frac{s^{*2}}{16a_e^{*2}}}\right) \qquad s^* \leq 4a_e^*$$

$$F_s^* = 1 \qquad s^* \geq 4a_e^*$$

$$F_e^* = \frac{6s^*}{\pi a_e^*}\frac{1}{4(a/a_e)^3-1} \qquad s^* \leq h^*$$

$$F_e^* = 1 + \frac{6}{\pi}\,\frac{\arcsin\frac{s-h^*}{2a_e^*} + \frac{s-h^*}{2a_e^*}\sqrt{1-\left(\frac{s-h^*}{2a_e^*}\right)^2}}{4(a/a_e)^3-1} \qquad h^* \leq s^* \leq h^*+2a_e^*$$

$$F_e^* = 1 \qquad s^* \geq h^*+2a_e^*$$

$$F^* = \frac{(4(a/a_e)^3-1)F_e^*+3F_s^*}{2(2(a/a_e)^3+1)} \qquad (6.10)$$

F^*_s, F^*_e release fraction for bubbles on small, large areas
s^* migration distance on large areas

From this, the effect of steady state bubble migration results as

$$\left(\frac{\dot{n}^*}{n^*}\right)_{migr} = \left(\frac{\dot{b}^*}{b^*}\right)_{migr} = - K^* \frac{9}{4\sin\pi/4(2(a/a_e)^3+1)} \frac{r^*}{a_e} \qquad (6.11)$$

(6.11) replaces (4.13) and must be inserted in (4.3), (4.30), and (4.32).

The last change in formulas for the grain face gas concerns the mean distance between grain face bubbles and intragranular bubbles needed for calculating creep by vacancy diffusion from the interior of the grain. Here, a in (4.25) is replaced by a_e:

$$2X = \frac{4a_e}{3+a_e S_l/r} \qquad (6.12)$$

This is correct for spherical grains and a good approximation for elongated ones, where the majority of grain face bubbles sit on the long sides of the grain and thus have a distance $2a_e$ instead of 2a from the next surface across the grain.

C. Gas in porosity

The different grain geometry only affects the total length of grain edges per grain, which is now

$$X_t = 4\pi a_e \left(\frac{1-P}{3}\right)^{3/2} (2+(a/a_e)^3)$$

and with this, (5.16) becomes

$$L_p = \frac{9\bar{x}}{2\pi a_e} \left(\frac{3}{1-P}\right)^{3/2} \frac{1}{2+(a/a_e)^3} \qquad (6.13)$$

7. Gas in Molten Fuel

The model for gas behaviour in molten fuel has not been changed appreciably from the one reported earlier /1/ and needs updating especially in two respects: Modeling of the gradual transition from solid to liquid phase - currently, the fuel is assumed to be molten as soon as the solidus is reached; and a more realistic model for coalescence between large and small bubbles, taking into account the diversion of the fluid flow around large bubbles /26/.

As it stands now, the model for molten fuel assumes, that three groups of bubbles exist upon melting: The former intragranular and grain face bubbles, and those formed from gas residing in the open and closed pores. These bubbles are assumed to reach instantly their equilibrium volume - given by the surface tension of the fluid - and their equilibrium rise velocity caused by buoyancy. The time constant for reaching the equilibrium has been previously estimated to be negligibly small /1/ for both processes. Before starting the calculation, bubble sizes in the three groups are checked; if the radii of any two groups differ by less than a factor 2, the groups are collapsed into one.

The following processes are modeled:

A. Precipitation and resolution of resolved gas.
B. Biased bubble migration, leading to coalescence and release, caused by buoyancy.
C. Random bubble movement due to Brownian motion, causing bubble coalescence /26/.

One bubble group is fully characterized by its gas contents and number density; for ℓ groups, there are thus 2ℓ differential equations to be solved. Release is excluded from these equations and treated at bigger time intervals. If bubbles pertaining to the same group coalesce, the product bubble is assumed to remain in the group; if the coalescing bubbles belong to different groups, the product is assumed to remain in the group of larger bubbles. If the groups are ordered according to size, starting with the smallest bubbles, the equations for group i read:

$$\dot{n}_i = - \sum_{j=i}^{\ell} G_{ij}$$

$$\dot{b}_i = - \sum_{j=i+1}^{\ell} G_{ij} \frac{b_i}{n_i} + P_i - R_i \qquad (7.1)$$

n_i number density of group i in molten fuel
b_i gas in bubble group i in molten fuel
G_{ij} coalescence rate for bubbles of group i with those of group j
P_i precipitation into group i bubbles
R_i resolution from group i bubbles

A. Precipitation and resolution

The two terms P_i and R_i from (7.1) are given by (see (3.6) and (3.7)):

$$P_i = 4\pi D_g^{\ell} n_i r_i c$$

$$R_i = \eta b_i \qquad (7.2)$$

r_i equilibrium radius of bubble group i
D_g^{ℓ} diffusion coefficient of atomic gas in molten fuel
c^{ℓ} gas resolved in molten fuel

$$c^{\ell} = \int_0^t \beta(t')dt' + c + c^* + b + b^* + b_p - \sum_{i=1}^{\ell} b_i(t) \qquad (7.3)$$

b_p gas in open and closed porosity at onset of melting.

The integral in (7.3) is to be taken over the time interval starting at the onset of melting; c, c*, b, and b* are the intragranular and grain face gas concentrations at onset of melting.

Thermal resolution is not being taken into account so far in (7.2).

B. Biased migration by buoyancy

Assuming Stokes' law holds, the bubble velocity caused by buoyancy is given by

$$v_i = \frac{2r_i^2 a_g}{9\nu} \tag{7.4}$$

v_i velocity of bubbles in group i
a_g acceleration of gravity
ν kinematic viscosity of molten fuel

From this and (3.17), (3.19), assuming the correction factor for bubble radius distribution equals unity, one derives

$$G^b_{ii} = \frac{4\pi}{9}\frac{a_g}{\nu} r_i^4 n_i^2$$

$$G^b_{ij} = \frac{2\pi}{9}\frac{a_g}{\nu} (r_i+r_j)^2(r_j^2-r_i^2)n_i n_j \tag{7.5}$$

If either the bubbles in one group grow very big ($r > 8 \cdot 10^{-3}$cm), or the void fraction grows big, (7.4), i.e. Stokes' law, does not hold any more. In addition, (3.17) and (3.19) do not take into account the divergence of flow around large bubbles. So far, no effort has been made to insert more realistic equations for these cases.

C. Random migration due to Brownian motion

The bubble diffusion coefficient due to Brownian motion is given by /27/:

$$D_i = \frac{kT}{6\pi\nu\rho_\ell r_i} \tag{7.6}$$

ρ_ℓ density of molten fuel

With (7.6), (3.18), (3.20), and again a correction factor of unity for the influence of bubble size distribution, the contribution of random bubble migration is

$$G_{ii}^{r} = \frac{4}{3}\frac{kT}{\nu\rho} n_i^2$$

$$G_{ij}^{r} = \frac{2}{3}\frac{kT}{\nu\rho}(r_i+r_j)\left(\frac{1}{r_i}+\frac{1}{r_j}\right) n_i n_j \qquad (7.7)$$

The total coalescence rate in (7.1) is

$$G_{ij} = G_{ij}^{b} + G_{ij}^{r} \qquad (7.8)$$

The integration of (7.1) is performed with the technique employed before the onset of melting. User defined time intervals are given with fuel temperature, gas production rate, and internal pressure of the pin varying linearly. These intervals are divided into subintervals that are automatically reduced in length with growing bubble velocity. Equations (7.1) are integrated for one subinterval with the Runge-Kutta-method employed for the intragranular and grain face equations; afterwards the release fraction is calculated with, simply

$$s_i = \int_0^t v_i(t')dt'$$

$$F_i = s_i/d \qquad s_i \leq d$$

$$= 1 \qquad s_i \geq d \qquad (7.9)$$

s_i migration distance in group i
F_i release fraction of bubbles in group i
d mean migration distance till release

where t is the time since onset of melting. d is to be supplied by the user. Swelling is given by

$$S^m = \frac{4\pi}{3} \sum_{i=1}^{\ell} n_i r_i^3 (1-F_i) \qquad (7.10)$$

S^m swelling of molten fuel

The calculation is finished when swelling exceeds 100 %, or when the bubbles are fully released. In the first case, continuation of the calculation is meaningless, since most assumptions, on which the above equations are based, break down.

8. Material Constants and Code Verification; Conclusions

For the material constants employed by LAKU measured values are used as far as possible, but many of them are not accurately known. In addition, since the LAKU-model employs a number of approximations, and since some physical processes, e.g. the release mechanism for intragranular gas during transients are at present controversial, some adjustment of parameters to fit measurements of gas release and swelling is indispensable. Nevertheless, care has been taken to remain within the limits of measured values.

The set of material constants currently employed by LAKU is summarized in Table 1. Though they are quite numerous, only a few are important for fitting, since results depend only weakly on many. The most sensitive parameters are

- for the irradiation part: Intragranular atomic gas diffusion coefficient and resolution constant;
- for the transient part: Bubble surface diffusion coefficient.

Many of the parameters listed in Table 1 are default values that may be replaced by the user. However, the calculations to be presented in the following have all been made with this set of constants. They were derived by analyzing, for the irradiation part, the results of numerous gas release measurements performed by Zimmermann /28/. Comparisons of his measurements and recalculations with LAKU are shown in Fig. 5 for probes with uniform temperatures, and in Fig. 6 for pin sections characterized by a mean temperature. The transient part has not had to be refitted recently; though a number of experiments under transient conditions have been performed recently, the current value of the surface diffusion coefficient is based on a recalculation of a summary of out-of-pile experiments performed early on by Randklev and Hinman /29/. A comparison of their results and LAKU recalculations, employing the newest version of LAKU, is shown in Fig. 7.

Recently, the code has been used to analyze some experiments of the older and newer FD-series performed by Sandia Laboratories; the results have been reported elsewhere /43/. There will be further analyses of out-of-

pile and in-pile experiments in the near future, which may entail some slight variations of parameters to achieve optimum results for all cases considered. Bigger changes of modeling are not planned at present, but some smaller changes may be warranted. Some of them were mentioned in the text already:

- Modeling of the different kinds of grain face bubbles under transient conditions (original lenticular and released spherical bubbles).
- Improved model for release from open pores under transient conditions accounting for the presence of macroscopic cracks.
- Release of gas by formation of microcracks under thermal shock conditions.
- Modeling of the gradual transition from solid to liquid state.
- Improved model for coalescence between large and small bubbles in molten fuel.

LAKU is, even without these improvements, a very comprehensive code that models all processes related to steady state and transient fission gas behaviour. At present, the discussion on the mechanism of transient gas release from the grains remains unresolved. In this respect, LAKU is among the great majority of codes, that assume an enhanced gas bubble migration mechanism as opposed to the thermal resolution mechanism modeled in the SINGAR-code /44/. If this latter mechanism is supported by experimental findings, the model in LAKU would have to be changed accordingly. In addition, the model for gas behaviour in molten fuel needs some more refinement. Apart from this, no major changes or additions are foreseen for the model.

Future work will concentrate on the formulation of simplified models suitable for insertion into bigger code systems. As has been mentioned in the introduction, a first step in this direction has been made already with the development of the coupled code URANUS-LAKU /17/. The version of LAKU used for this retains the modeling described here with only a few simplifications and some additional numerical approximations. Numerical results differ by a few percent at the most from those of the stand-alone version; computer times are about a factor 3 lower, i.e. are of the order of 10 - 20 seconds for one cross section of a pin for a full irradiation +

transient simulation on an IBM 3033. This is still a little high, but nearly adequate for coupling with a stand-alone pin behaviour code like URANUS, but it is clearly not sufficient for insertion into a whole-core accident code modeling a big number of pins. Thus, a greatly simplified version remains to be developed.

Table of Symbols

a	radius of grain
a^*	radius of grain face
a_g	acceleration of gravity
a_o	grain radius of fabricated fuel
B	fraction of surface covered by grain face bubbles
B_{max}	maximum value of B
b/b^*	gas in intragranular / grain face bubbles
b_i	gas in bubble group i in molten fuel
C	parameter in high-temperature stress-strain relation
c/c^*	resolved intragranular / grain face gas
D_b/D_b^*	intragranular / grain face bubble diffusion coefficient
D_g/D_g^*	intragranular / grain face diffusion coefficient of atomic gas
D_g^ℓ	diffusion coefficient of atomic gas in liquid fuel
D_i	bubble diffusion coefficient due to Brownian motion in molten fuel, for bubble group i
D_s	surface diffusion coefficient
D_u/D_u^*	self diffusion coefficient of heavy species in grain / on grain face
F/F^*	fraction of bubbles released from grain / grain face
F_B	factor describing bubble radius dependence of grain face precipitation
F_i	release fraction of bubble group i in molten fuel
F_p	fraction of open pores
F_{vol}	ratio of grain face area to volume
f	intragranular relative loss rates due to sweeping and bubble migration (steady state)
g/g^*	gas released from grains / grain faces
g_{gb}/g_p	intragranular gas released to grain faces / porosity

H	parameter in high temperature stress-strain relation
H_s	vaporization energy of fuel
k	Boltzmann's constant
L	Avogadro's number
L_p	average number of links per pore
m	parameter in high temperature stress-strain relation
m_f	molecular number of fuel
m_g	atomic number of gas
n/n^*	number density in intragranular / grain face bubbles (per unit volume / surface area)
n_i	number density of bubble group i in molten fuel
n_p	number density of pores
n_p^c/n_p^o	number of closed / open pores
n_o	number density of intragranular bubble sites
P	fuel porosity (fabricated and restructured)
p	local hydrostatic pressure
p_{ex}/p^*_{ex} /p^{**}_{ex}	excess pressure in intragranular bubbles / grain face bubbles / closed pores
p_s	equilibrium vapour pressure of fuel
Q	source of gas released to open pores
Q_s	surface diffusion heat of transport
R	universal gas constant
r/r^*	radius of intragranular / grain face bubbles
r^{**}	radius of closed pore without tunnels
r^{**}_{eff}	effective radius of closed pore
r_c/r_o	radius of cylindrical tunnel attached to closed / open pore
r_f	radius of damage zone of fission spike
r_i	radius of bubbles in group i in molten fuel
r^{**}_p	effective radius of open porosity

r_z/r_z^* /r_z^{**}	cell radius for intragranular bubbles / grain face bubbles / closed pores
$S_1/S_2/S_3$	intragranular / grain face / porosity swelling
S^m	swelling of molten fuel
s/s*	migration distance of intragranular / grain face bubbles during transient
s_i	migration distance of bubbles in group i in molten fuel
T	temperature
∇T	bulk thermal gradient
∇T_s	thermal gradient at bubble surface
t	time into irradiation or transient or melting
u	superficial (Darcy) velocity
v/v*	intragranular / grain face bubble velocity
v_i	velocity of bubbles in group i in molten fuel
v_p	pore velocity
w	Van-der-Waals constant
x	radial coordinate
$\bar{x}$	average tunnel length
x_c/x_o	tunnel length for closed / open pore
α	geometrical factor for calculating the volume of lenticular bubbles
β/β^*	gas production rate / grain face gas source term
γ	surface tension of fuel
δ	width of grain face
ε	fraction of pore volume in unirradiated fuel going into tunnel formation
η	resolution constant
κ	permeability
λ	mean jump distance of surface atom
μ	viscosity of inert gases

ν	kinematic viscosity of molten fuel
ρ	density of gas in open pores
ρ_{ℓ}	density of molten fuel
σ	collision cross section of fuel vapour phase
ψ	contact angle of grain face bubble
Ω	molecular volume
Ω_{vir}	virtual volume assigned to gas atom resolved in grain face during transient

Literature

/1/ L. Väth: Current status of modeling fission gas behaviour in the Karlsruhe code LANGZEIT/KURZZEIT; KfK 2962 (1980)

/2/ K. Laßmann: URANUS, a computer programme for the thermal and mechanical analysis of the fuel rods in a nuclear reactor; Nucl. Eng. Design, 45 (1978), 325

/3/ J. Rest: GRASS-SST: A Comprehensive, Mechanistic Model for the Prediction of Fission-Gas Behavior in UO_2-Base Fuels during Steady-State and Transient Conditions; NUREG/CR-0202 (ANL-78-53), 1978

/4/ J. Rest, S.M. Gehl: The mechanistic prediction of fission-gas behavior during in-cell transient heating tests on LWR fuel using the GRASS-SST and FASTGRASS computer codes; Transactions of the 5th international conference on structural mechanics in reactor technology, Berlin, 13.8.1979, Vol. C1/6

/5/ R.W. Ostensen: FISGAS - A code for fission gas migration and fuel swelling in an LMFBR accident; NUREG/CR-1124 (SAND78-1790), 1979

/6/ I.R. Brearley, D.A. MacInnes: An improved equation of state for inert gases at high pressures; Journ. Nucl. Mat. 95 (1980), 239

/7/ C. Baker: The migration of intragranular fission gas bubbles in irradiated uranium dioxide; Journ. Nucl. Mat. 71 (1977), 117

/8/ W. Chubb, W. Storhok, D.L. Keller: Observations relating to the mechanisms of swelling and gas release in uranium dioxide at high temperatures; Journ. Nucl. Mat. 44 (1972), 136

/9/ C. Ronchi: Physical processes and mechanisms related to fission gas swelling in MX-type nuclear fuel; Journ. Nucl. Mat. 84 (1979), 55

/10/ F.S. Ham: Theory of diffusion-limited precipitation; Journ. Phys. Chem. Solids 6 (1958), 335

/11/ R.S. Nelson: The stability of gas bubbles in an irradiation environment; Journ. Nucl. Mat. 31 (1969), 153

/12/ J.A. Turnbull: The distribution of intragranular fission gas bubbles in UO_2 during irradition; Journ. Nucl. Mat. 38 (1971), 203

/13/ J.R. Matthews, M.H. Wood: An efficient method for calculating diffusive flow to a spherical boundary; Nucl. Eng. Des. 56 (1980), 439

/14/ L. Väth: Approximate treatment of the grain-boundary loss term in fission gas release models; Journ. Nucl. Mat. 99 (1981), 324

/15/ E.E. Gruber: A generalized parametric model for transient gas release and swelling in oxide fuels; Nucl. Technol. 35 (1977), 617

/16/ K. Maschke, H. Overhof, P. Thomas: A note on percolation probabilities; phys. stat. sol. (b) 60 (1973), 563

/17/ T. Preußer, L. Väth: to be published

/18/ G.W. Greenwood, A.E.J. Foreman, D.E. Rimmer: The role of vacancies and dislocations in the nucleation and growth of gas bubbles in irradiated fissile material; Journ. Nucl. Mat. 4 (1959), 305

/19/ J.R. Hofmann, C.C. Meek: Internal pressurization in solid mixed-oxide fuel due to transient fission gas release; Nucl. Sci. Eng. 64 (1977), 713

/20/ C.S. Olsen: UO_2 pore migration and grain growth kinetics, SMiRT-5, Berlin, Vol. C, 1979

/21/ S.B. Ainscough, B.W. Oldfield, J.O. Ware: Isothermal grain growth kinetics in sintered UO_2 pellets; Journ. Nucl. Mat. 49 (1973/4), 117

/22/ F.A. Nichols: Transport phenomena in nuclear fuels under severe temperature gradients; Journ. Nucl. Mat. 84 (1979), 1

/23/ H. Blank: Fission fragment re-solution mechanisms; Proceedings of the Workshop on Fission Gas Behaviour in Nuclear Fuels, Karlsruhe, 26.-27.10.1978 (EUR-6600EN), p. 307

/24/ J.A. Turnbull, C.A. Friskney: The release of fission products from nuclear fuel during irradiation by both lattice and grain boundary diffusion; Journ. Nucl. Mat. 58 (1975), 31

/25/ D.H. Worledge: Fuel fragmentation by fission gases during rapid heating; SAND80-0328 (1980)

/26/ E.A. Fischer: private communication

/27/ L.D. Landau, E.M. Lifshitz: Fluid Mechanics; Pergamon Press, London, 1959

/28/ H. Zimmermann: Fission gas release and fission gas retention in oxide fuels; Proceedings of the Workshop on Fission Gas Behaviour in Nuclear Fuels, Karlsruhe, 26.-27.10.1978 (EUR-6600EN), p. 35

/29/ E.H. Randklev, C.A. Hinman: Fission gas behavior in mixed-oxide fuel during overpower and thermal transient tests; International Conference on Fast Breeder Reactor Fuel Performance, Monterey, Calif., 5.-8.3.1979 (HEDL-S/A--1552-FP; CONF-790306--24)

/30/ Hj. Matzke: Rare gas diffusion in ceramic nuclear fuels; Proceedings of the Workshop on Fission Gas Behaviour in Nuclear Fuels, Karlsruhe, 26.-27.10.1978 (EUR-6600EN), p. 337

/31/ E.A. Fischer: Analysis of experimental fission gas behaviour data in fast reactor fuel under steady state and transient conditions; KfK 2370 (1977)

/32/ J.R. Matthews: Mechanical properties and diffusion data for carbide and oxide fuels; AERE-M-2643 (1974)

/33/ R.J. DiMelfi, L.W. Deitrich: The effects of grain boundary fission gas on transient fuel behavior; Nucl. Technol. 43 (1979), 328

/34/ O.D. Slagle: Deformation behavior of UO_2 above 2000°C; HEDL-TME 79-37 (1979)

/35/ W. Beeré, G.L. Reynolds: The morphology and growth rate of interlinked porosity in irradiated UO_2; Journ. Nucl. Mat. 47 (1973), 51

/36/ E.N. Hodkin: The ratio of grain boundary energy to surface energy of nuclear ceramics as determined from pore geometries; Journ. Nucl. Mat. 88 (1980), 7

/37/ J.K. Fink, M.G. Chasanov, L. Leibowitz: Thermophysical properties of uranium dioxide; Journ. Nucl. Mat. 102 (1981), 17

/38/ R.W. Weeks, R.O. Scattergood, S.R. Pati: Migration velocities of bubble-defect configurations in nuclear fuels; Journ. Nucl. Mat. 36 (1970), 223

/39/ B.J. Buescher, R.O. Meyer: Thermal-gradient migration of helium bubbles in uranium dioxide; Journ. Nucl. Mat. 48 (1973), 143

/40/ P. Nikolopoulos, S. Nazare, F. Thümmler: Surface, grain boundary and interfacial energies in UO_2 and UO_2-Ni; Journ. Nucl. Mat. 71 (1977), 89

/41/ J.A. Turnbull, R.M. Cornell: The re-solution of fission-gas atoms from bubbles during the irradiation of UO_2 at an elevated temperature; Journ. Nucl. Mat. 41 (1971), 156

/42/ J.R. Matthews, M.H. Wood: Modelling the transient behaviour of fission gas; Journ. Nucl. Mat. 84 (1979), 125

/43/ L. Väth: Experience from recalculations of experiments on transient fission gas behaviour with the Karlsruhe model LAKU; Proceedings of the International Specialist Meeting on Fission Gas Behaviour in Safety Experiments, Cadarache, 5.-7.10.1983 (to be published)

/44/ D.A. Macinnes, I.R. Brearley: A model for the release of fission gas from reactor fuel undergoing transient heating; Journ. Nucl. Mat. 107 (1982), 123

Appendix

Input description

The input is unformatted and will be listed with the following notation: Kx: start new card; Sx: logical decision or branch. Variables, whose names start with I-N are integer, all others are real.

S1	for a restart run K15, otherwise K2	
K2	TITLE	problem identification, up to 8 alpha-numerical characters
K3	NPRINT	0: no output 1: short output 2: long output
	NZONE	number of radial nodes ($\leq$ 20)
	NTIME	number of irradiation time intervals
	NVARY	0: default values for material constants >0: number of material constants to be changed from default value
	A	>0: as fabricated grain diameter [cm] 0.: $2a = 9 \cdot 10^{-4}$
	P	>0: as fabricated porosity 0.: P = .1
K4	(R(I),I=1, NZONE+1)	radii of nodes [cm]
S5	for each irradiation time interval K6 - K10, then S11	
K6	TS	length of interval [d]
	PO	initial pressure [g/cms^2]
	PT	final pressure [g/cms^2]
K7	(T(I),I=1, NZONE+1)	temperatures at radial zone boundaries [C]
K8	(BETA(I),I= 1,NZONE)	fission gas creation rate [mole/cm^{3}s]
S9	if NVARY > 0, insert NVARY cards K10 after K8 for the first time step; otherwise proceed to S5	
K10	IND	index of constant to be changed
	VALUE	new value of constant

The following values of IND are possible:

IND=1 Type of EOS. Normally, the reduced Van-der-Waals EOS is used (VALUE=1.). With VALUE=2., the hard-sphere EOS is utilized.

=2 ψ [°], contact angle of grain face bubbles

=3 GA1 } surface tension γ [g/s²]:
=4 GA2 } γ = GA1+GA2·T [K]

=5 DSSM } surface diffusion coefficient D_s
=6 DSSE } [cm²/s]:
D_s=DSSM·exp(-DSSE/T[K])

=7 DHM } intragranular diffusion coefficient
=8 DHR } for atomic gas D_g [cm²/s]:
=9 DIRR } D_g=DHM exp(-DHR/T[K])+DIRR·β[mole/cm³s]

=10 QS surface diffusion heat of transport Q_s [gcm²/s²]

=11 BMAX maximum fraction of grain face covered by bubbles

=12 FACT factor for calculating grain face diffusion coefficient for atomic gas, f*

=13 ETO: resolution constant [s^{-1}]:
η = ETO·β[mole/cm³s] /2.9·10^{-11}

=14 ENBO: number density of intragranular bubble sites [cm^{-3}]

The default values are listed in Table I

S11 for creation of a restart file K12, otherwise S13

K12 'FILE' constant

S13 for calculation of transient continue with K14, for new irradiation calculation K2, for end of calculation, K24

K14 'TRANS' constant

K15 NEXPER 1: cooling and cutting before transient
0: otherwise

NITMAX maximum number of pressure iterations

NRAND 0: fuel in contact with cladding
1: otherwise

NTIME number of time intervals for transient

DRMAX maximum radial step length for pressure calculation ($\leq$ .05) [cm]

D migration distance in molten fuel till release [cm]

TMELT fuel melt temperature [C]

PO initial pressure [g/cms²]

K16	(XKAP(I), I=1,NZONE)	fuel permeability [cm^2]
K17	(TO(I),I=1, NZONE+1)	initial temperatures at radial zone boundaries [C]
K18	(BETAO(I), I=1,NZONE)	initial fission gas creation rate [$mole/cm^3s$]
S19	for each time interval K20 - K22, then S23	
K20	DTT	length of interval [s]
	N	number of sub-intervals for output ($\geq$ 1)
	P1	pressure at end of interval [g/cms^2]
K21	(T1(I),I=1, NZONE+1)	temperatures at radial zone boundaries for end of interval [C]
K22	(BETA1(I), I=1,NZONE)	fission gas creation rate at end of interval [$mole/cm^3s$]
S23	for new calculation K2, otherwise K24	
K24	'END'	constant.

Control cards

One control card for unit number 20 is needed in case the restart option is used. A dataset containing the FORTRAN-listing of the programme is kept on disk; for information on the newest version, please contact the author.

Input example

A simple test example is listed below. The cross section of the pin is subdivided into two zones. Standard grain sizes, porosities, and material constants are employed. One 50 day irradiation interval is followed by a 6s transient leading to melting. The results of the irradiation calculation are reserved for calculating further transients.

```
'TESTCASE'
2   2   1   0   0.   0.
0.   .18751   .25
50.   5.+6   5.+6
```

```
2550.    1350.    825.
2*2.77-11
'FILE'
'TRANS'
1    4    1    2    .06    .5    2840.    2.+6
6.67-15    1.-13
3*1640.
2*0.
5.    5    2.+6
2840.    2640.    2440.
2*0.
1.    .2    2.+6
3*2940.
2*0.
'END'
```

Table 1: Material constants employed in LAKU

Constant		Numerical value		Literature
$a(t)$	radius of grain: growth formula	$a^4 = a_o^4 + t[s] \cdot 1.075 \cdot 10^{-4} \cdot \exp(-46548/T[K])$ $a \leq .1115 \exp(-7620/T[K])$	cm^4	/20,21/
B_{max}	maximum fraction of grain face covered by bubbles	.8		
D_g	intragranular diffusion coefficient for atomic gas	$.03 \exp(-45280/T[K])$ $+2.6 \cdot 10^{-5} \beta\ [mole/cm^3 s]$	cm^2/s	/30/
$D_g^* = f^* D_g$	grain face diffusion coefficient for atomic gas	$f^* = 100$		
D_s	surface diffusion coefficient	$5.7 \cdot 10^5 \exp(-54400/T[K])$	cm^2/s	/31/
D_u	self diffusion coefficient of heavy species in grain	$2 \exp(-55600/T[K])$	cm^2/s	/32/
D_u^*	self diffusion coefficient of heavy species in grain face	$.1262 \exp(-35470/T[K])$	cm^2/s	/33/

Table 1 continued (1)

Constant		Numerical value		Literature
D_b	steady state bubble diffusion coefficient	$\frac{3 \cdot 10^{-19}}{r^2} \exp(-45000/T[K])$	cm^2/s	/3/
H_s	vaporization energy of fuel	10^{-11}	gcm^2/s^2	/37/
m_f	molecular number of fuel	270		/38/
m_g	atomic number of gas	132		/38/
n_o	number density of intragranular bubble sites	10^{16}	cm^{-3}	
p_s	equilibrium vapor pressure of fuel	$5.943 \cdot 10^{14} \exp(-72034/T[K])$	g/cms	/37/

Table 1 continued (2)

Constant		Numerical value		Literature
C, H, m	high temperature creep law	$\dot{\varepsilon}_e = \sigma_e^{3.5} \cdot 8.84 \cdot 10^{-9}$ exp(-150966/T[K]) ($T \geq 2700$) $\dot{\varepsilon} = \sigma_e^{4.5} \cdot 1.43 \cdot 10^{-30} \cdot$ exp(-66425/T[K]) ($T < 2700$) (σ [g/cms])	s^{-1}	/34/
Q_s	surface diffusion heat of transport	$6.95 \cdot 10^{-12}$	gcm^2/s^2	/15/
r_f	radius of damage zone of fission spike	$5 \cdot 10^{-7}$	cm	/23/
w	Van-der-Waals constant	49.26	cm^3/mole	/31/
γ	surface tension of fuel	1527.-.3457T [K]	g/s^2	/40/
δ	width of gain face	$5 \cdot 10^{-8}$	cm	/35/

Table 1 continued (3)

Constant		Numerical value		Literature
ϵ	fraction of pore volume in unirradiated fuel going into tunnel formation	.15		
η	resolution constant	$6 \cdot 10^{-4} \cdot (\beta\ [\mathrm{mole/cm^3 s}] / 2.9 \cdot 10^{-11})$	s^{-1}	/41/
λ	mean jump distance of surface atom	$1.12 \cdot 10^{-6}$	cm	/15/
μ	viscosity of inert gases	$.00018(T[K]/300.)^{1/2}$	g/cms	/19/
ν	kinematic viscosity of molten fuel	.0051	cm^2/s	/37/
ρ_ℓ	density of molten fuel	8.8	g/cm^3	/37/
σ	collision cross section of fuel vapour phase	$3.85 \cdot 10^{-15}$	cm^2	/39/
ψ	contact angle of grain face bubble	50°		/36/
Ω	molecular volume	$4.08 \cdot 10^{-23}$	cm^3	/38/

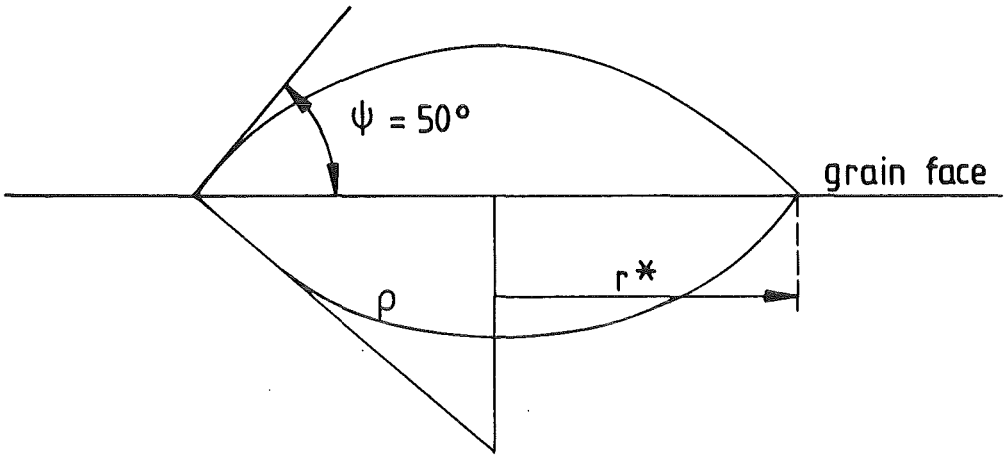

Fig.1: Grain face bubble (ρ : radius of curvature)

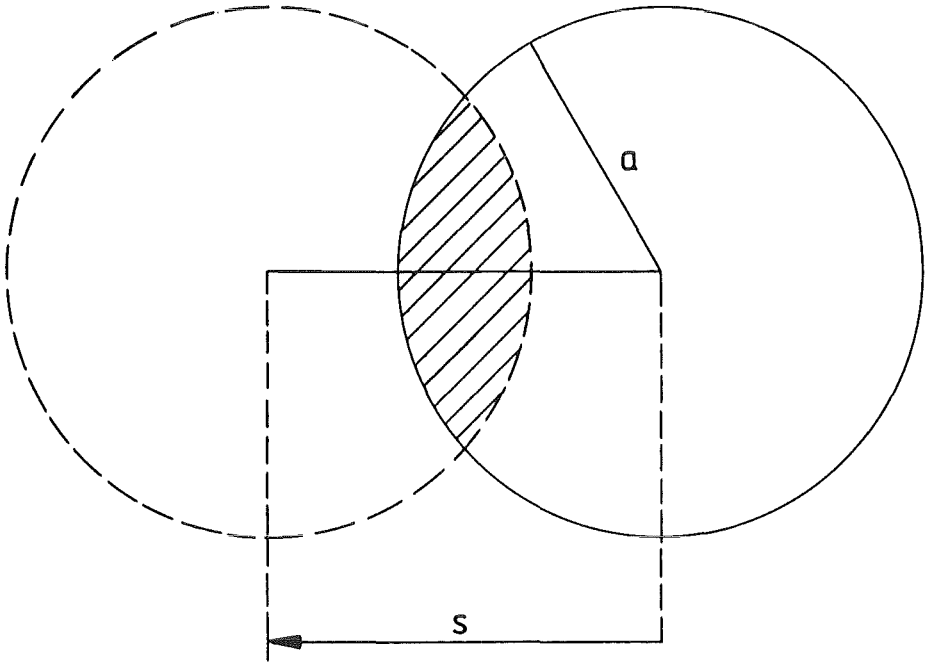

Fig.2: Illustration of gas release by bubble migration. Right circle: grain with radius a; left circle: virtual position of bubbles after traveling distance s; shaded area: fraction of unreleased bubbles

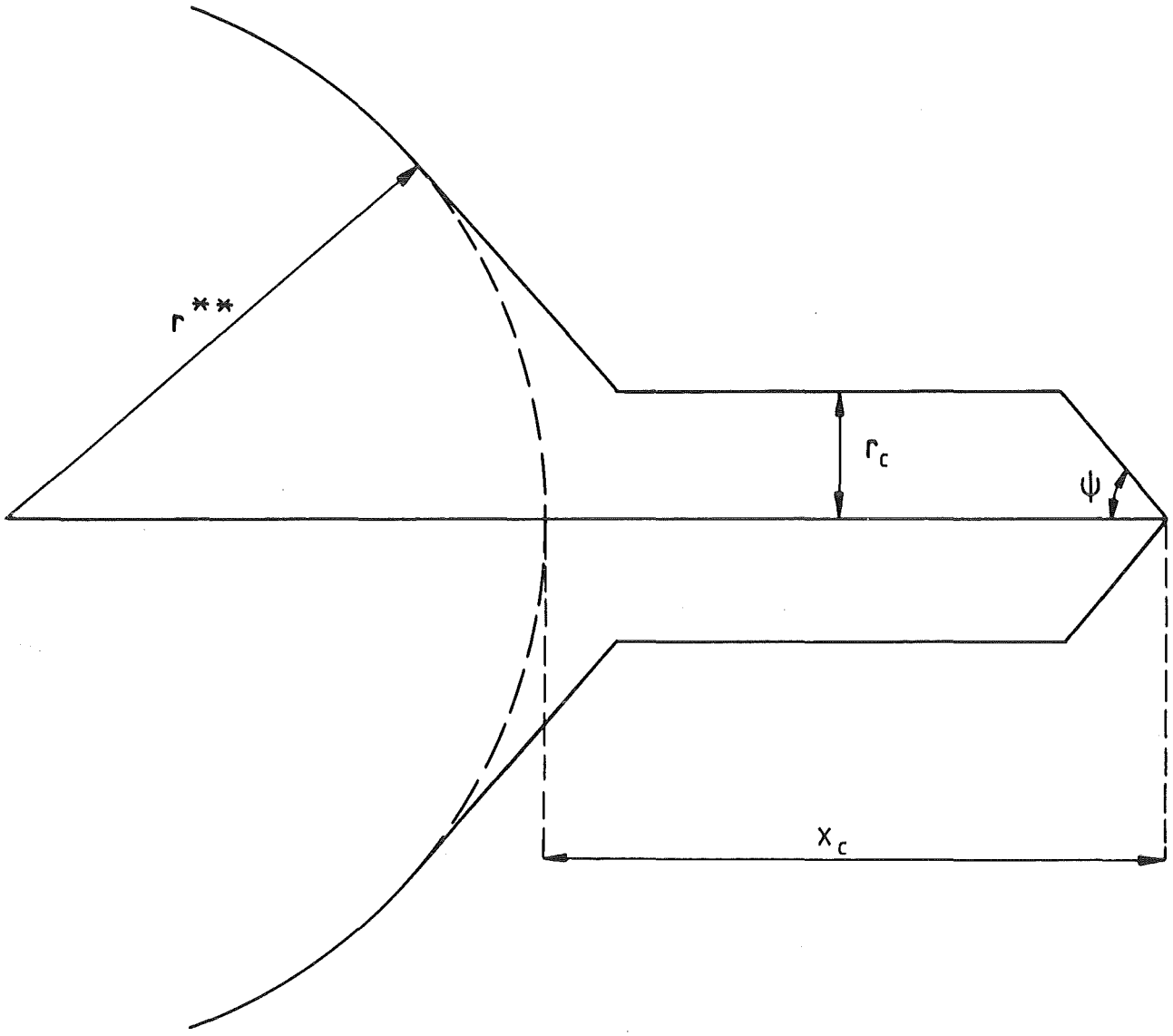

Fig. 3 : Model geometry of pore and tunnel

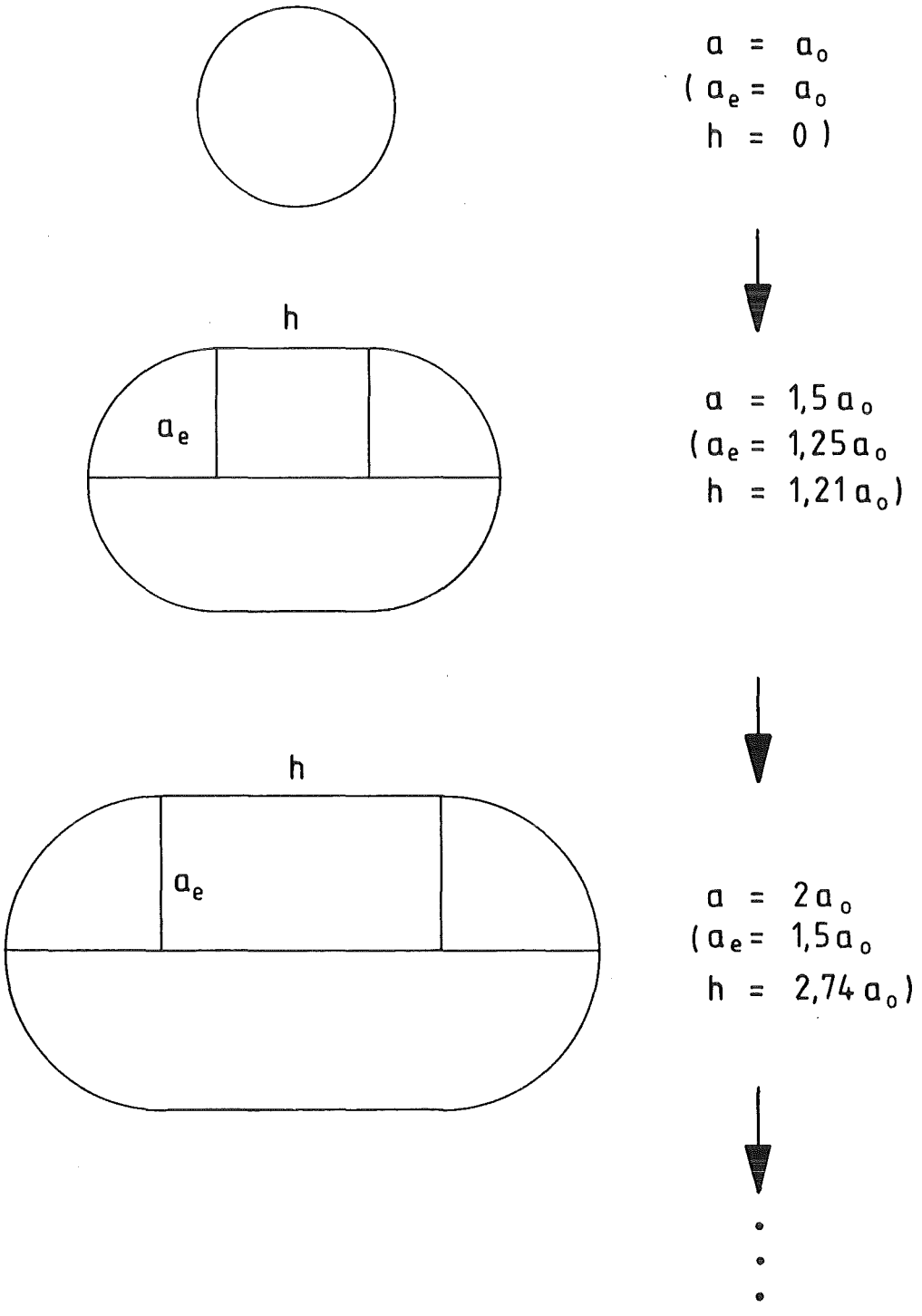

Fig. 4 : Geometric model for evolution of elongated grains

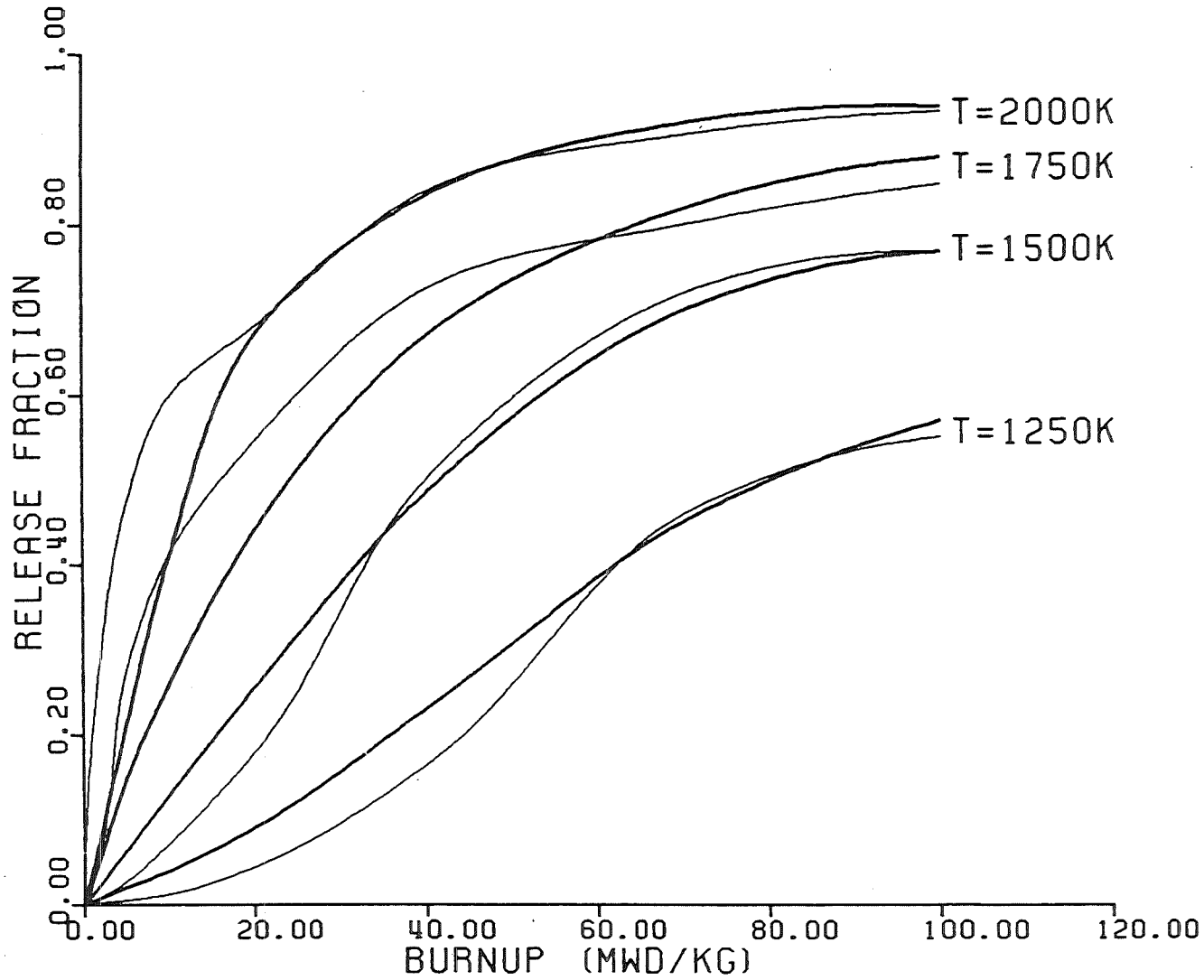

FIG. 5: GAS RELEASE DURING IRRADIATION FØR SMALL PRØBES
(— EXP. RESULTS BY ZIMMERMANN; — LAKU RECALCULATIØN)

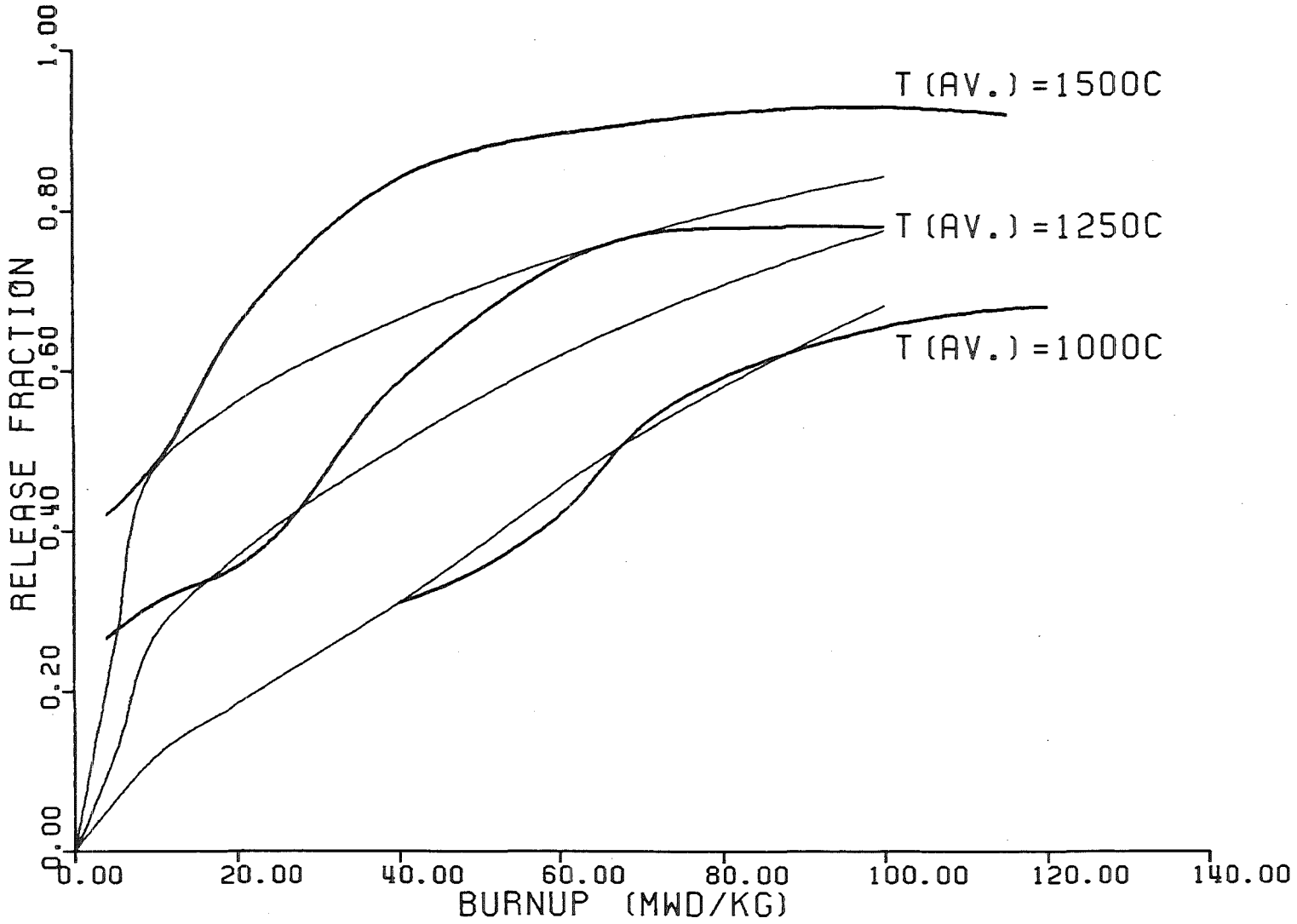

FIG. 6: GAS RELEASE DURING IRRADIATION FØR PINS
(— EXP. RESULTS BY ZIMMERMANN; — LAKU RECALCULATION)

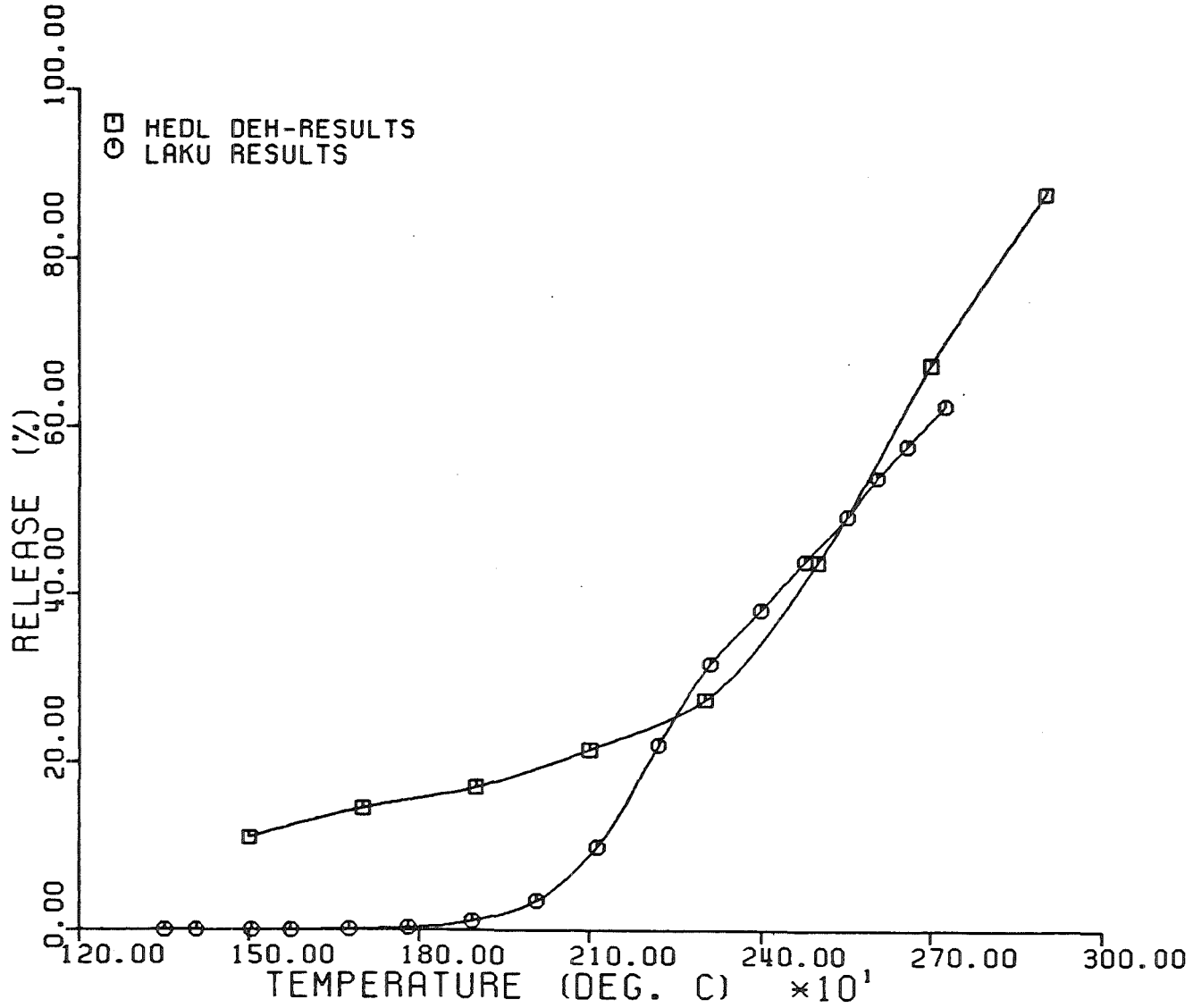

FIG. 7: SUMMARY OF HEDL DEH-EXPERIMENTS

Acknowledgement

I would like to thank Mr. E. Fischer for many helpful discussions and for reviewing the manuscript, and Mrs. G. Bunz for her careful typing.